ISTANBUL TECHNICAL UNIVERSITY ★ GRADUATE SCHOOL OF SCIENCE ENGINEERING AND TECHNOLOGY

PRODUCTION OF CARBON NANOTUBE REINFORCED NANOPREPREGS AND THEIR CHARACTERIZATION

M.Sc. THESIS

Beyza BOZALİ

Department of Textile Engineering

Textile Engineering Programme

JUNE 2018

ISTANBUL TECHNICAL UNIVERSITY ★ GRADUATE SCHOOL OF SCIENCE ENGINEERING AND TECHNOLOGY

PRODUCTION OF CARBON NANOTUBE REINFORCED NANOPREPREGS AND THEIR CAHARACTERIZATION

M.Sc. THESIS

Beyza BOZALİ

Department of Textile Engineering

Textile Engineering Programme

Thesis Advisor: Asst. Prof. Elif OZDEN YENIGUN

JUNE 2018

ISTANBUL TEKNİK ÜNİVERSİTESİ ★ FEN BİLİMLERİ ENSTİTÜSÜ

KARBON NANOTÜP TAKVİYELİ NANOPREPREGLERİN GELİŞTİRİLMESİ VE KARAKTERİZASYONU

YÜKSEK LİSANS TEZİ

Beyza BOZALİ
503151829

Tekstil Mühendisliği Anabilim Dalı

Tekstil Mühendisliği Programı

Tez Danışmanı: Dr. Öğr. Üye. Elif ÖZDEN YENİGÜN

HAZİRAN 2018

Beyza BOZALİ, a MSc. student of ITU Graduate school of Science Engineering and Technology student ID 503151829, successfully defended the thesis entitled "PRODUCTION OF CARBON NANOTUBE REINFORCED NANOPREPREGS AND THEIR CHARACTERIZATION", which she prepared after fulfilling the requirements specified in the associated legislations, before the jury whose signatures are below.

Thesis Advisor:	**Asst. Prof. Elif OZDEN YENIGUN** ISTANBUL Technical University	.....
	Prof. Emel ÖNDER KARAOĞLU ISTANBUL Technical University	.....
	Assoc. Prof. Fevzi Ç. CEBECİ SABANCI University	.....

.

Date of Submission : 04.05.2018
Date of Defence : 08.06.2018

To my family,

FOREWORD

Since I started preparing my thesis, first and foremost I would like to thank to my supervisor Asst. Prof. Elif Ozden Yenigün and Assoc. Prof. Hulya Cebeci for their valuable insights and directions gave me needful guidance to complete and write this thesis. Besides my friends and colleagues in Nanomaterials, Textiles and Advanced Composites Research Group in Aerospace Research Center, from Istanbul Technical University, I would also thank to my family that have always supported me throughout my MSc study.

This thesis is supported by 116M427 numbered TUBITAK project supported entitled "Production of vertically aligned carbon nanotube reinforced nanoprepregs and their use in thermoplastic composites for reinforcing interface". Also, I would like to thank ITU AYP-2016-12 project for providing material support and conference funding. I also would like to thank Universal Textile Center for access of mechanical testing facilities.

July 2018

Beyza BOZALİ

(Textile Engineer)

TABLE OF CONTENTS

Page

FOREWORD ..... **ix**
TABLE OF CONTENTS ..... **xi**
ABBREVIATIONS ..... **xiii**
LIST OF TABLES ..... **xv**
LIST OF FIGURES ..... **xvii**
SUMMARY ..... **xxi**
ÖZET ..... **xxiii**
1. INTRODUCTION **1**
1.1 Motivation 2
1.2 The Novelty of Thesis 3
2. LITERATURE REVIEW **5**
2.1 Thermoplastic Laminated Composites 5
2.2 Reinforcing Strategies in Laminated Composites 6
2.3 The Role of Nanofibers in Interface Toughening 8
2.4 The Role of Nanomaterials in Interface Toughening 11
2.4.1 CNTs as a reinforcing element in interface toughening 12
2.4.2 CNTs reinforced thermoplastic-based laminated composites 16
2.5 High Performance Polymers with Potential Use in Thermoplastic Composites 19
3. MATERIALS AND METHOD **21**
3.1 Materials 21
3.2 Experimental Road Map of This Thesis 21
3.3 Fabrication of PBI Nanofibers by Electrospinning 22
3.3.1 Randomly oriented PBI nanofiber production 23
3.3.2 Aligned PBI nanofiber production using home-built wire drum 25
3.4 Doping of Fe^{+3} Catalysis onto Nanofibers 25
3.4.1 Immersion technique for Fe^{+3} catalysis 26
3.4.2 Dip-coating technique for Fe^{+3} catalysis 27
3.5 Chemical Vapor Deposition (CVD) for CNTs Production 28
3.5.1 Fabrication of PBI/CNTs nanocarpets 29
3.5.2 Synthesis of CNTs onto PBI nanofibrous substrates 29
3.5.3 The material selection and fabrication of thermoplastic nanoprepregs interleaved with PBI/CNTs nanoprepregs 31
3.6 Characterization of PBI Nanofibers, PBI/CNTs Nanocarpets and Thermoplastic PBI/CNTs Nanoprepregs 34
3.6.1 Characterization methods used for PBI nanofibers 34
3.6.2 Characterization methods used for PBI/CNTs nanocarpets 36
3.6.3 Characterization methods used for thermoplastic nanoprepregs 38
4. RESULTS AND DISCUSSION **39**
4.1 Results for Neat PBI Nanofiber 39

4.1.1 Morphological analysis of randomly oriented and aligned PBI electrospun nanofibers 39
4.1.2 Effect of Fe^{+3} catalysis concentration on the PBI nanofiber surface morphologies 43
4.1.3 Monitoring surface morphologies of neat and Fe^{+3} doped aligned PBI nanofibers by optical microscope 45
4.1.4 Elemental analysis on Fe^{+3} doped PBI nanofibers 46
4.1.5 Mechanical performance of randomly and aligned PBI nanofiber 47
4.1.6 Thermal degradation of PBI nanofibers 47
4.2 Characterization on PBI/CNTs Nanocarpets 48
4.2.1 Raman analysis of CNTs quality for PBI/CNTs nanocarpets 48
4.2.2 Thermal degradation of PBI/CNTs nanocarpets 50
4.2.3 Morphological analysis for PBI/CNTs nanocarpets with SEM 50
4.2.4 Electrical conductivity performance of PBI/CNTs nanocarpets 54
4.2.5 CNTs grown on PBI based commercial fabric 55
4.3 Characterization on Thermoplastic Nanoprepregs 57
4.3.1 Tensile properties 57
5. CONCLUSIONS 59
REFERENCES 61

ABBREVIATIONS

PBI	: Polybenzimidazole
DMF	: N, N-dimethylformamide
DMAc	: Dimethylacetamide
PES	: Poly (ether sulphone)
PS	: Polysulphone
PS	: Polysulphone
PA6	: Polyamide 6
PP	: Polypropylene
PMMA	: Poly (methyl methacrylate)
GF	: Glass Fiber
CF	: Carbon Fiber
PEI	: Polyetheylenimine
PEEK	: Poly (ether ether ketone)
ABS	: Acrylonitrile Butadiene Styrene
CVD	: Chemical Vapor Deposition
SWCNT	: Single Wall Carbon Nanotube
MWCNT	: Multi Wall Carbon Nanotube
SEM	: Scanning Electron Microscopy
TGA	: Thermal Gravimetric Analysis
EDX	: Energy Dispersive X-Ray Analysis
CED	: Cohesive Energy Density
ENF	: End Notch Flexure
DCB	: Double Cantilever Beam
3Pb	: 3 Point Bending

LIST OF TABLES

Page

Table 2.1: Literature review which nanofibers used as toughening element. 11
Table 2.2: Physical properties of CNTs. 12
Table 3.1: Electrospinning process parameters for the production of randomly oriented nanofibers. 24
Table 3.2: Solubility parameters of thermoplastic polymers. 32
Table 4.1: Tensile properties of aligned and randomly oriented PBI nanofiber. 47
Table 4.2: Electrical conductivity results. 55

LIST OF FIGURES

Page

Figure 1.1 The change in viscosity versus temperature for thermoset and thermoplastic polymers [2]. 1
Figure 1.2: The synergetic effect of CNTs and PBI nanofibers, addressing the novelty of proposed approach. 4
Figure 2.1: Z-pins integrated into laminated composite [12]. 6
Figure 2.2: Reinforcement in laminated composites. 7
Figure 2.3: Particle and film interleaved laminated composites [19]. 8
Figure 2.4: Basic electrospinning principle [20]. 9
Figure 2.5: Collector assemblies for the production of aligned nanofibers. 9
Figure 2.6: Potential applications of CNTs [37]. 12
Figure 2.7: Schematic view of SWCNTs and MWCNTs [20]. 13
Figure 2.8: (a) Arc discharge method (b) Laser ablation technique (c) CVD [38]... 14
Figure 2.9: Schematic view of interaction between catalyst and substrate affecting growth of SWCNTs [48]. 15
Figure 2.10: CNTs growth mechanisms: (a) tip-growth model, (b) base-growth model [50]. 16
Figure 2.11: A-CNTs as nano-stitching elements onto fiber [52]. 17
Figure 2.12: Aligned CNTs onto alumina fiber [52]. 18
Figure 2.13: Chemical structure of PBI polymer. 19
Figure 2.14: PBI-silica nonwoven. 20
Figure 3.1: Experimental road map of this thesis. 22
Figure 3.2: (left) Schematic of electrospinning step-up with rotate drum (top) and home-built wire drum (bottom) and (right) SEM images of randomly oriented (top) and aligned PBI nanofibers (bottom). 23
Figure 3.3: a) Polymer solution kept at oil bath b) Rotate drum mounted on Argeteknolab® electrospinning device. 24
Figure 3.4: Electrospinning setup with mounted home-built wire drum. 25
Figure 3.5: a) Schematic view of immersion technique b) Catalyst process of PBI nanofibers with immersion technique. 26
Figure 3.6: Dip-coating of PBI nanofiber produced at 15wt% using 50 mM catalysis concentration. 27
Figure 3.7: a) Coating of randomly oriented PBI nanofibers produced at 15wt% using 50 mM catalysis solution. 27
Figure 3.8: Randomly oriented PBI nanofiber produced at 15wt% immersed into 50 mM catalysis solution. 28
Figure 3.9: a) Commercial PBI fabric placed into acetone b) Immersion of PBI fabric in 50 mM catalysis solution. 28
Figure 3.10: CVD system used in ITUARC exhibiting a) Heater, b) PLC, c) Mass flow controller, d) Reactor furnace. 29

Figure 3.11: Illustration of CVD set-up. 30
Figure 3.12: CVD growth protocol revealing time-temperature relation in each step. 31
Figure 3.13: PBI monomer. 31
Figure 3.14: a) PES, b) PEI and c) PS Monomer. 32
Figure 3.15: Hot press used for nanoprepreg production. 33
Figure 3.16: a) PES granules b) PES thin film formed by hot press. 33
Figure 3.17: Nanoprepreg laminate stacking. 34
Figure 3.18: Measurement of nanofiber diameters by using ImageJ software a) Uploading image into the program, b) Defining of measurement scale-bar, c) Calculation of diameters by image processing. 35
Figure 3.19: Characteristic peaks of MWCNTs [71]. 37
Figure 3.20: 4 point probe electrical conductivity instrument. 38
Figure 3.21: UTM device exhibiting tensile specimens mounted with pneumatic tensile jaws. 38
Figure 4.1: Optical image of 22wt% PBI nanofiber. 39
Figure 4.2: SEM image of PBI nanofibers produced at 15wt% and histogram revealing fiber diameters. 40
Figure 4.3: SEM image of PBI nanofibers produced at 20wt% and histogram revealing fiber diameters. 40
Figure 4.4: SEM image of PBI nanofibers produced at 22wt% and histogram revealing fiber diameters. 41
Figure 4.5: a) Randomly oriented and b) Aligned PBI nanofibers produced at 20wt% concentration. 42
Figure 4.6: a) Aligned PBI nanofibers produced at 20wt% concentration b) The histogram revealing the degree of alignment. 42
Figure 4.7: 15wt% randomly oriented PBI nanofiber morphology and its fiber diameter histogram. 43
Figure 4.8: a) Fe^{+3} doped with 5 mM solution randomly oriented PBI nanofibers produced at 15wt% and b) histogram revealing fiber diameter distribution. 44
Figure 4.9: a) Fe^{+3} doped with 5 mM solution randomly oriented PBI nanofibers produced at 15wt% and b) histogram revealing fiber diameter distribution. 44
Figure 4.10: Optical microscope images of aligned PBI nanofibers at 20wt% collected at a) 1 hour b) 4 hour and c) 8 hour. 45
Figure 4.11: Optical microscope images of Fe^{+3} doped aligned PBI nanofibers at 20wt% collected at a) 1 hour b) 4 hour and c) 8 hour. 46
Figure 4.12: EDX analysis of 50 mM deposited onto 15wt% PBI nanofiber Fe^{+3} doped aligned PBI nanofibers at 20wt%. 46
Figure 4.14: TGA analysis of neat PBI nanofiber produced at 15wt%. 47
Figure 4.15: Raman analysis of CNTs growth on 15wt%, 20wt% and 22wt% PBI nanofiber immersed in 50 mM catalysis solution. 49
Figure 4.16: Raman analysis of CNTs growth on 15wt%, 20wt% and 22wt% PBI nanofiber immersed in 80 mM catalysis solution. 49
Figure 4.17: Thermogravimetric analysis for PBI/CNTs nanocarpets. 50

Figure 4.18: a) Randomly oriented PBI nanofiber b) CNTs grown on aligned PBI nanofiber c) Aligned PBI nanofiber d) CNTs growth on a single aligned PBI nanofiber as a zoomed view. 51
Figure 4.19: (top) SEM micrographs of CNTs grown on randomly oriented PBI nanofibers using 5 minute growth time (bottom) CVD protocol exhibiting time and temperature in each step. 52
Figure 4.20: (top) SEM micrographs of CNTs grown on randomly oriented PBI nanofibers using 8 minute growth time (bottom) CVD protocol exhibiting time and temperature in each step. 53
Figure 4.21: (top) SEM micrographs of CNTs grown on randomly oriented PBI nanofibers using 15 minute growth time (bottom) CVD protocol exhibiting time and temperature in each step. 53
Figure 4.22: CNTs growth onto nanofiber. 54
Figure 4.23: (left) PBI nanofiber (right) PBI/CNTs nanocarpet. 55
Figure 4.24: a) Optical microscope image of image of commercial fabric with the composition of 59% P-aramid/ 40% PBI/1% anti-static (left), SEM images revealing unsuccessful growth on image of commercial fabric with the composition of 59% P-aramid/ 40% PBI/1% anti-static (right) b) Optical microscope image of image of commercial fabric with the composition of 58% P-aramid/ 40% PBI/2% anti-static (left), SEM images revealing unsuccessful growth on image of commercial fabric with the composition of 58% P-aramid/ 40% PBI/2% anti-static (right). 56
Figure 4.25: SEM images of a) Fe^{+3} doped PBI/Aramid blended fibers b) CNTs grown PBI/Aramid blended fibers. 56
Figure 4.26: a) Neat PES film b) PBI nanofiber interlayered PES nanoprepreg c) PBI/CNTs interlayered PES nanoprepreg. 57
Figure 4.27: Neat PES film, PBI/PES and PBI/CNTs/PES nanoprepreg stress-strain graph. 58

PRODUCTION OF CARBON NANOTUBE REINFORCED NANOPREPREGS AND THEIR CHARACTERIZATION

SUMMARY

Epoxy based thermoset prepregs has been dominated materials market particularly in the automotive and aerospace applications. However, thermoplastic polymers recently have drawn attention with their potential to overcome challenges such as long cure cycles, poor fracture toughness, low viscosities, limited shelf lives and non-recyclability of thermosets. Thermoplastic resins have offered several advantages including recyclability, high impact resistance, and high thermal stability.

Reinforcement strategies in laminated composites included both matrix and interface toughening. For matrix toughening, dispersion of additives into the matrix has been the most preferred method. One of the disadvantages of this method is stemming from non-proper dispersion of nanomaterials in the matrix. Moreover, the increase in polymer viscosity associated to nanomaterials reduced polymer processability. Interface toughening in laminated composites could be in the form of film, particle, and nanofibers to hinder crack propagation and improve better load transfer between each plies. With the use of interface elements in thermoplastic laminated composites, the superior properties could be enhanced and transferred to overall composites.

Carbon nanotubes (CNTs) are hollow structures in which graphite layers are placed in cylinder forms. The superior properties of CNTs is dependent on CNTs physical properties, chirality, and the number of walls. In the case of interlaminar toughening CNTs could be placed through different routes such as buckypaper interleaving, CNTs grown on fibers. In most of bucky paper applications, CNTs were dissolved in an appropriate solvent. However, the use of any solvents would significantly form low-volume fraction CNTs structures, and also not are not permitted in aerospace applications. In order to overcome these challenges, new methods have been studied, which embraced the synthesis of CNTs structures on fiber substrates. By direct growth of CNTs onto fiber surface enabled the integration of high volume fraction CNTs into structure. Besides, CNTs morphology and orientation could be precisely controlled.

Interfacial interaction between polymer and reinforcing element promoted the effective load transfer mechanisms benefiting either micromechanical interlocking, chemical bonding or Van der Waals bonding. The interaction between CNTs and polymer provided an increase in interfacial shear strength and contributed to the overall structure' performance under different loadings.

In this thesis, a novel method to grow CNTs on polymeric nanofibrous substrates and to fabricate their thermoplastic nanoprepregs interleaved by these hierarchical nanocarpets was proposed. The growth of CNTs on polybenzimidazole (PBI) nanofibers were exploited to create conductive, strong and light weight interleaves. Nanofibers produced by electrospinning were optimized and catalysed with iron nitrate solutions containing transition metals providing carbon diffusion and solubility. As coating method to dope catalyst, immersion and dip-coating techniques were preferred.

These different coating methods were assessed based on their ability to distribute transition metals onto nanofiber. The chemical vapour deposition (CVD) for the growth of CNTs was preferred due to its advantages such as; CNTs orientation control and high quality of CNTs. With the use of ethylene, helium and hydrogen gases, CNTs growth protocol was optimized. The orientation control of CNTs could be enhanced by aligned nanofibers as substrates. PBI/CNTs nanocarpets were then used as interleaves for the production of thermoplastic nanoprepregs. Thermoplastic nanoprepregs were prepared and characterized as potential interlayer element in laminated composites.

The morphology, thermal stability and overall quality of CNTs were determined by SEM, TGA and Raman spectroscopy respectively. From morphological analysis, revealed that randomly oriented PBI nanofibers could not enable vertically aligned CNTs growth due to homogenously accumulated Fe^{+3} ions over nanofiber surface. I_g/I_d ratio interpreted from Raman analysis was determined as ≈1 which referred as successful production of high quality CNTs grown onto nanofiber.

The electrical conductivity of PBI/CNTs nanocarpets was calculated by 4 point probe conductivity instrument. Conductivity values of randomly oriented and aligned PBI/CNTs nanocarpets were 1.56±0.6 S/cm and 1.2±0.5 S/cm, respectively. The difference in the conductivity could be attributed to the reduced contact resistance between carbon nanotubes and well intersected CNTs network.

The tensile performance of PBI/CNTs/PES nanoprepregs showed that tensile strength of PBI/CNTs/PES nanoprepregs was 412±13 MPa, where PBI/PES nanoprepregs had a tensile strength of 348±5 MPa. With the addition of CNTs onto nanofiber, tensile strength of nanoprepregs was enhanced by 18%. The reason behind this increase was mechanical interlocking and good load transfer between CNTs and PES resin.

KARBON NANOTÜP KATKILI NANOPREPREG ÜRETİMİ VE KARAKTERİZASYONNU

ÖZET

Günümüz ileri teknoloji uygulamalarında epoksi reçine esaslı termoset prepreg kullanımı özellikle havacılık ve otomotiv uygulamalarında ön plana çıkmaktadır. Fakat termoset reçinelerin uzun kürlenme reaksiyonları, zayıf kırılma dayanımları, düşük viskoziteleri, kısıtlı raf ömrü ve geri dönüştürülemez olmaları termoplastik reçinelere ilginin artmasına neden olmaktadır. Termoplastik reçinelerin sahip olduğu yeniden kalıplanabilme, yüksek darbe dayanımı ve kürlenme işlemlerinin olmaması tercih edilmelerini sağlamaktadır.

Lamine kompozitlerde takviye metotları hem matris geliştirme hem de ara yüzey iyileştirmeyi kapsamaktadır. Matris dayanımını arttırmak için katkı malzeme disperse edilerek ekleme en çok uygulanan yöntemlerden biridir. Bu yöntemin dezavantajlarından biri nanomalzemenin düzgün bir şekilde matris içinde dağılamamasıdır. Dağılmama problemiyle nanomalzemelerin bir araya toplanma eğilimi göstermeleri, dağıtmanın sağlanması için uygulanan yöntemlerle nanomalzemelerin sahip oldukları üstün özelliklerin yitirilmesine neden olmaktadır. Ayrıca polimer viskozitesindeki artış matrisin işlenebilirliğini azaltmaktadır. Katmanlı kompozitte ara yüzey iyileştirmek için ara yüzeye, katmanlar arasında mekanik kitlenmelere, çatlak ilerlemeyi önleyecek ve yük transferini sağlayacak film, parçacık veya nanofiber gibi yapıların eklenmesiyle çeşitli yüklemeler altında performans artışı sağlanmaktadır. Nanomalzemelerin özellikle termoplastik yapılarda kullanımı, nanomalzemelerin sahip olduğu üstün mekanik, elektrik ve termal özelliklerinin yapıya aktarımına olanak sağlamaktadır.

Karbon Nanotüp (KNT) grafit tabakalarının silindir halinde yerleştiği içi boş yapılardır. Sahip oldukları üstün performans özellikleri KNT'nin fiziksel özellikleri, kiralliği, duvar sayısıyla ilişkilendirilir. KNT'lerin ara yüzey iyileştirmede kullanımı, bucky paper, fiber üzerinde KNT büyüterek matrise entegrasyonunun sağlanması yöntemlerini kullanarak gerçekleştirilebilmektedir. Pek çok buckypaper uygulamalarında ise uygun çözücü içinde KNT dağıtılır. Çözücü kullanımı düşük oranlarda KNT oluşumuna neden olmakla birlikte, havacılık sektörü içinde uygun olmamaktadır. Bu problemleri ortadan kaldırmak adına yeni yöntemler üzerine çalışmalar yapılarak KNT yapılarının yapıya katkılanması sağlanmıştır. Bu yöntemlerin en önemlilerinden biri KNT yapılarının çeşitli üretim yöntemleriyle fiber üzerinde sentezi gerçekleştirilerek kontrollü olarak kompozit içerisine entegrasyonu sağlanır. Fiber üzerinde büyütme ile yüksek hacim oranlarında KNT'lerin yapıya katılımı sağlanabilmektedir. Bu şekilde KNT yapısının morfolojisi ve yönelimi kontrol edilebilmektedir.

KNT ve polimer arasındaki ara yüzey güçlendirmesi mikromekanik kitlenme, kurulan kimyasal bağ veya Van der Waals bağları ile sağlanan efektif yük transferi ile sağlanır. Nano malzeme ve matris arasındaki etkileşim ara yüzey kayma mukavemetini

arttırmakla birlikte yapının farklı yüklemeler altında mekanik performansının artmasına sebep olur.

Bu çalışmada önerilen yüksek degredasyon sıcaklığına sahip PBI nanoliflerin KNT altyapısı olarak kullanılarak termoplastik reçineye emprenye edilmesidir. PBI nanoliflerin üzerinde KNT büyütülmesi ile iletken, güçlü ve hafif ara elemanların üretimi gerçekleşecektir. Üretilecek olan nanolifler elektro-dokuma yöntemiyle hazırlanarak, KNT üretimi için katalizlenerek KNT üretimi için karbon çözünürlüğünü ve difüzyon kabiliyetini arttıracak geçiş metallerinin nanolif üzerine kaplanması sağlanmıştır. Kataliz derişimi ve polimer molekül ağırlığı değiştirilerek parametrik çalışma yapılmış ve sonuçları listelenmiştir. Katalizleme yöntemleri olarak batırma ve daldırmalı kaplama yöntemleri tercih edilerek katalizin nanolif üzerinde aynı oranda dağılımının sağlanması amaçlanmıştır. Farklı katalizleme yöntemleri geçiş metallerinin nanolif üzerine dağılımına fayda sağlayacaktır.

KNT üretim metodu olarak kimyasal buhar biriktirme yöntemi diğer yöntemlere kıyasla KNT kontrolünün sağlanması, yüksek kalitede KNT üretimi gibi avantajlarından dolayı tercih edilmiştir. KNT üretimi sırasında kullanılan etilen, hidrojen ve helyum gazları optimize edilmiştir. KNT yönelimi alt yapı olarak sıralı PBI nanoliflerinin kullanılmasıyla geliştirilebilir. Üretilen PBI/KNT yapıları lamine kompozitlerde ara katman olarak kullanımını sağlamak için termoplastik reçineye sıcak baskı yöntemiyle emprenye edilerek ince filmler halinde üretilmiştir. Filmler halinde üretilen termoplastik nanoprepreglerin lamina kompozit uygulamalarında ara yüzey olarak kullanılarak ara katman mekanik dayanımın artıracağı düşünülmektedir.

Nano boyutta PBI nanolif altyapı üzerinde KNT büyütme çalışmalarına paralel olarak ticari olarak temin edilen kumaşlarından çözgü yönündeki iplikler liflerine ayrılarak KNT büyütme çalışmaları yapılmıştır. Dolayısıyla, nanolif üretimi için kullanılan protokol ile μm boyutunda PBI esaslı lifler radyal dağılımın elde edilebileceği öne çıkmıştır.

KNT morfolojisi, termal dayanımı ve genel özellikleri SEM, TGA ve Raman karakterizasyonlarıyla belirlenecektir. Morfolojik analizde, kataliz metalinin homojen olmayan şekilde gelişigüzel yerleşmiş nanolif üzerinde dağılması dikey yönelimli KNT üretimine engel olmuştur. Raman spektroskopisi ile belirlenen I_g/I_d oranı ≈1 civarında olması yüksek kalitede KNT üretildiğini göstermektedir. G ve D pikleri sırasıyla sp^2 atomlarının düzlem içi titreşimlerinin sp^3 bağlı atomlarının düzlem dışı hareketlerinin sonucudur. Bu oran grafit karbon yapısının bir ölçüsü olarak kabul edilebilir.

PBI/KNT nanohalıların elektrik iletkenlikleri 4 noktadan temas iletkenlik ölçer ile belirlenmiştir. Gelişigüzel yerleşmiş ve sıralı nanoliflerin iletkenlik değerleri sırasıyla 1,56±0,6 S/cm ve 1,2±0,5 S/cm olarak belirlenmiştir. Yönelimli PBI/KNT nanohalının elektrik iletkenlik değerlerinde görülen artışa karbon nanotüpler arasında meydana gelen temas direncinin azalmasının sebep olduğu düşünülebilir.

PES filmler arasına emprenye edilen PBI/KNT nanohalı yapılarının mekanik performans etkisi çekme testiyle ASTM D882-12 standartı takip edilerek belirlenmiştir. Çekme testi sonucunda rasgele KNT dağılımına sahip PBI/KNT/PES nanoprepreglerin kopma dayanımının 348±5 MPa olduğu, KNT içermeyen PBI/PES nanoprepreg kopma dayanımının 412±13 MPa olduğunu göstermiştir. KNT katkısının kopma dayanımını yaklaşık olarak %18 oranında arttırdığını ortaya koymuştur. Mekanik olarak bu artışın nedeni olarak, mekanik olarak KNT yapısının PES ile bağlantı oluşturarak etkin yük dağılımına izin vermesi olarak açıklanabilir. Sonraki

dönemde, yönelimli KNT'lerin PES matrisin mekanik davranışına olan katkısı da ayrıca incelenecektir.

1. INTRODUCTION

Thermoset resins have drawn great attention in composite industries by means of high thermal resistance, low process viscosity, and high fracture toughness. However, these resins had limited shelf lives and poor recyclability. So, new expectations have been risen from composite industry to drive thermoplastics' research while benefiting advantages such as short manufacturing cycles, easy storage, remoulding/reshaping ability and recyclability [1]. The main structural difference upon temperature change between thermosets and thermoplastic polymers were displayed in Figure 1.1. At low temperatures, both thermosets and thermoplastics behave as solids. When the temperature increased, there would be distinct viscosity profile change between thermosets and thermoplastics. While thermoplastics' viscosity decreased with the increase in temperature due to ease in chain movement, once thermoset materials started to be cross-linked, this irreversible reaction caused hindered polymer chains and viscosity increased.

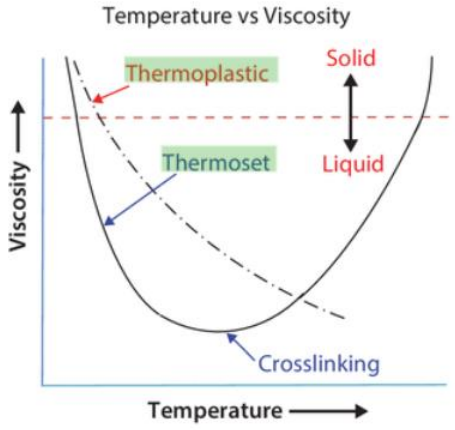

Figure 1.1 The change in viscosity versus temperature for thermoset and thermoplastic polymers [2].

Thermoplastic polymers usually combined with different type of fillers as reinforcement such as particles, nanoparticles, and fibers, could be used in structural composites as in the form of laminated or sandwich composites to improve mechanical and thermal properties of overall structure. For the preparation of particulate reinforced

polymers, as mostly preferred approach, different sized particles were dispersed in resin. Related to the nature of interaction between reinforcing particulate and polymer, mechanical, thermal or electrical performance could be enhanced or depressed.

Unlike particulates, due to their high aspect ratio fibers exhibit different characteristics than bulk material in polymer composites. When the interfacial contacted between fiber and polymer resin was successfully achieved in manufacturing, non-creep behaviour of fibers could be transferred into polymer and visco-elastic property of thermoplastics could be improved. Mostly carbon, glass, graphene, boron fiber *etc* had been mostly used reinforcing elements in thermoplastic composites [3].

Apart from conventional fiber and particles as reinforcements in thermoplastic polymers, nanomaterials such as clay, carbon nanotubes (CNTs), graphene *etc*. have been drawn attention as potential nanosized reinforcing elements [2].

1.1 Motivation

The main aim of this thesis is to produce thermoplastic nanoprepregs by impregnating CNTs grown polymeric nanofibers into thermoplastic resins, which is later explored as an interlayer element to reinforce thermoplastic based laminated composites. With the proposed method, it is possible to incorporate CNTs at the interface in a controlled architecture, which also allows to improve both mechanical and electrical properties. With the demand of recyclable and repairable composites, aerospace industry strongly is seeking out new material systems for laminated composites. This thesis sets out to answer how conductive and strong interlayer elements can be produced to reinforce thermoplastic laminated composites without sacrificing their recyclability.

- First, a novel method of growing random and vertically aligned CNTs onto polymeric fibrous network is proposed. Polybenzimidazole (PBI) nanofibers are produced by electrospinning and later used as a substrate in CNTs growth process. There are no previous studies reported which describes the production of CNTs on polymeric fibers, unlike metal [4], alumina [5] and silicon substrates [6].
- The CNTs synthesis protocol on polymeric nanofibrous is explored by discussing the effect of nanofiber orientation. Hence, randomly oriented and

aligned PBI nanofibers are produced by electrospinning and used as substrate for CNTs growth, which can sustain to CNTs synthesis temperatures.

- The effect of catalysis concentration on the quality of CNTs production is discussed by monitoring the length and orientation of CNTs.
- PBI/CNTs nanocarpets are then impregnated into thermoplastic PES films to produce PBI/CNTs nanoprepregs and their contribution to mechanical and electrical properties is systematically examined.

1.2 The Novelty of Thesis

This thesis brings these following contributions to knowledge:

- The synthesis of randomly oriented and vertically aligned CNTs onto polymeric nanofiber system is a novel approach, which benefits uniform 3D stress distribution of nanofibers as substrate on the overall composites. This approach eliminates further substrate removal and ease keeping structural integrity and handling for further processes.
- The electrical conductivity achieved through tuning CNTs architecture without adding weight penalty enables multifunctionality and control on conduction mechanism.
- Using PBI nanofiber system as a substrate for CNTs growth is a unique way of creating PBI/CNTs nanocarpets as multifunctional interleaves. This is possible only if the nanofiber system can withstand high temperatures. High thermal degradation temperature ($\approx 750^{\circ}C$) of PBI polymer helps to keep its structural integrity after CNTs growth process, which assists one-step integration to form nanoprepregs.
- PBI/CNTs nanocarpets can be transferred to structural composites by eliminating additional dispersion/integration steps due to their free-standing.
- In each steps, material systems are characterized in terms of their mechanical and electrical properties and reported to exploit their unique nature.

Synergetic effect of CNTs and PBI nanofibers by emphasizing manufacturing methods in this thesis is illustrated in Figure 1.2**:**.

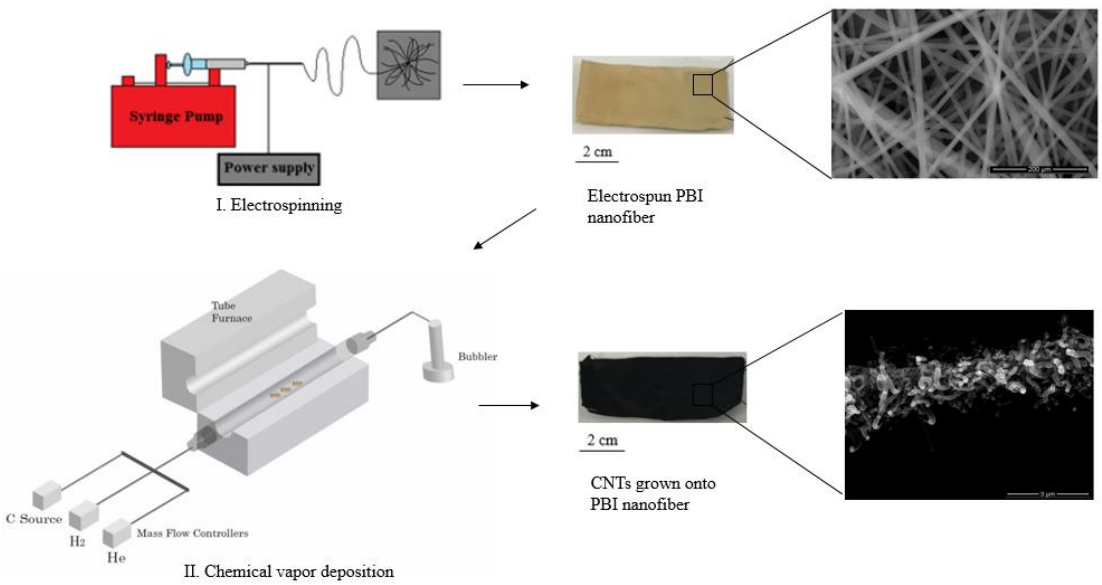

Figure 1.2: The synergetic effect of CNTs and PBI nanofibers, addressing the novelty of proposed approach.

2. LITERATURE REVIEW

2.1 Thermoplastic Laminated Composites

Thermoplastic resin-based laminated composites capable of remolding/reshaping ability, recyclability, and multifunctionality had been drawn attention in the composite industry. Thermoplastic polymers contained chemically independent macromolecules within the structure and multiple cycles of heating-cooling could be applicable to the structure that gave the property of reproducibility and recyclability to the thermoplastic polymers. The main advantages of thermoplastic polymers over thermosets were the easy processability without any use of chemical additives and crosslinking reactions [7].

Thermoplastic laminated composites generally consisted of differently sequenced unidirectional or bi-directional fiber prepregs which were formed by stacking plies with heating. A stack of differently numbered plies made of a various type of materials placed in different orientation occurred in laminated composites. Bonding of each ply was accomplished by the curing procedure of the resin dependent on the type of material used. The response of the structure under loading was different for both each lamina and overall laminate structure depending on the stacking sequence and the ply number [8].

High-performance polymers such as PEEK, PEI had a high usage area in thermoplastic laminated composites. Polyetheretherketone (PEEK) was a semi-crystalline polymer used in thermoplastic laminated composites as in the form of glass reinforced or carbon reinforced since it had a tough, rigid structure, good creep structure, and fatigue behavior. Diez-Pascual et al. reported that in the case of polysulfone (PS) compatibilized SWCNT/PEEK composites, since PS increased the tube-tube resistance, conductivity decreased, but with the increase of CNT volume fraction within SWCNT/PEEK composites, conductivity enhanced above percolation threshold [9]. Especially carbon fiber reinforced PEEK laminated composites were the great advantage of high-performance elements because of its high strength to weight

and modulus to weight ratios [10]. Also their strength and stiffness could not be affected by the temperature increase over to 150˚C while most of the polymers were thermally degraded at these temperatures.

2.2 Reinforcing Strategies in Laminated Composites

There were different failure modes in laminated composites such as delamination, debonding, matrix cracking, *etc*. Delamination which occurred in the presence of poor interfacial strength between plies was the most common failure mode in the case of laminated composites due to the low fracture toughness in the direction of through-thickness. To hinder through-thickness delamination within laminates, there were different routes carried out so far such as matrix toughening, z-pinning, braiding, 3D weaving, stitching, tufting, interleaving subphases into interface *etc*. [11]. In order to decrease the delamination between plies in laminated composites, pinning in the through thickness direction (also known as z-pinning) could be applied as one of the reinforcing strategies in interlaminar toughening. By the conduction of z-pinning within the interface (z-pins were the small diameter rods integrated into the interface between plies), the overall mechanical performance of laminated composites could be enhanced with the presence of generated friction and adhesion between plies. Hindering of crack propagation at the thickness direction places was achieved by locking movement of the plies by z-pins as shown in Figure 2.1.

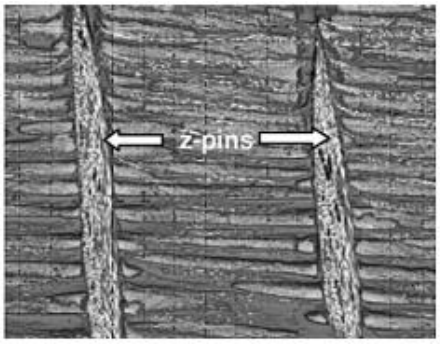

Figure 2.1: Z-pins integrated into laminated composite [12].

Another reinforcement route was multi-dimensional braiding which provided resistance to micro-cracking and delamination. By braiding one graphite layer into another one, the mechanical enhancement was established. Braided construction showed good stability under impact loading and had enhanced damage tolerances when compared with regular laminated composites [13].

Interface toughening was a critical state in laminated composites affected by the type of materials, toughening mechanism and strength occurred between plies. Interlaminar toughening could be accomplished with interleaving since interface regions at laminated composites were the weakest parts in the case of mechanical performance. In order to increase the overall performance of interlayer toughening, either matrix toughening or inclusion of crack hindering nanomaterials between laminates could be established [3]. There were different reinforcement mechanisms in laminated composites such as particle/filler interleaving, film interleaving and electrospun nanofiber interleaving as shown in Figure 2.2*:* [14].

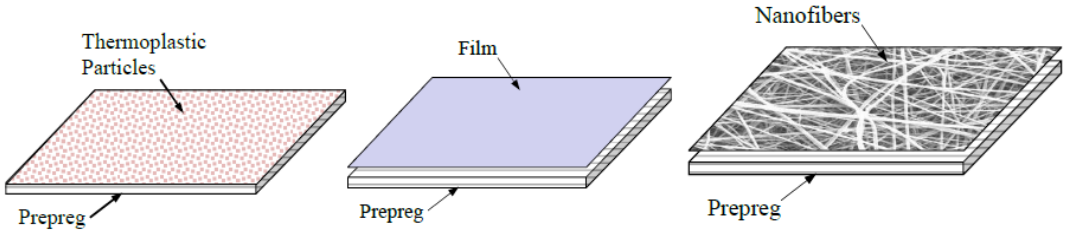

Figure 2.2: Reinforcement in laminated composites.

The main drawback of the nanomaterial inclusion between plies was the low rate of dispersibility which induced weak points and crack spots within interface leading failures under various types of loading. In a study reported by Stevanovic et al., thermoplastic acrylonitrile butadiene styrene (ABS) particles used as a matrix toughened element in laminated composites and interaction between matrix and particle enhanced mechanical performance of the laminates [15].

Yasaece et al., investigated the effect of different type of films including thermoplastic film, fiber reinforced tape and chopped aramid fibers on interlaminar toughness and reported enhanced properties in fracture toughness [16, 17]. In another study reported by Hojo et al., by interleaving thermoplastic particles and ionomer based resin films, Mode-I delamination resistance was evaluated within carbon fiber reinforced epoxy laminated composites as shown in Figure 2.3. Kevin and Sue investigated the contribution of CNTs into polyamide-12 (PA) epoxy thin film as an interlayer in composites which was manufactured by vacuum assisted resin transfer moulding (VARTM) and fracture toughness of the composite. Remarkable increase in Mode II crack initiation was exhibited with the addition of CNTs into the overall composite structure [18].

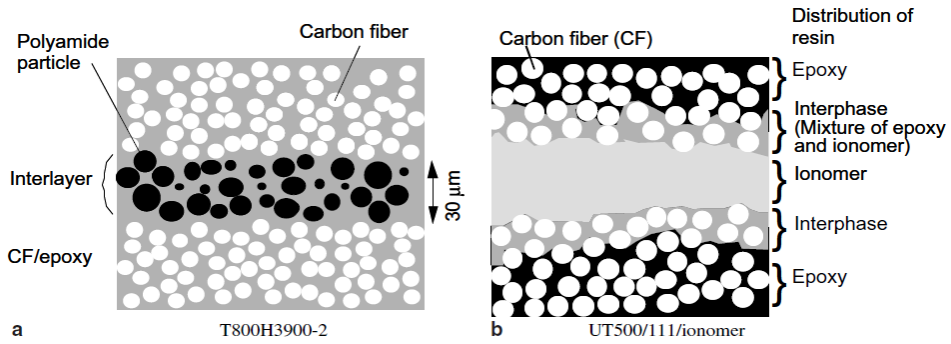

Figure 2.3: Particle and film interleaved laminated composites [19].

2.3 The Role of Nanofibers in Interface Toughening

Since particle interleaving leaded to decrease in-plane mechanical properties and film interleaving caused an increase in laminate thickness, the use of nanofibers as interleaves increased the toughening performance of laminated composites. The aim of nanofiber interleaving into laminated composites was to provide superior bonding and damage tolerance between adjacent plies. Advantages of the high surface area and high porosity of nanofibers made nanofibers ideal interface toughening elements in laminated composites.

The interest in nanofiber production by electrospinning process had attracted remarkable attention due to the production of ultra-thin fibers with diameters as small as 10 nm to micron-scale, low-cost, and versatility. Besides the aforementioned qualities of the process, it also provided continuous nanofiber production which was used in different application fields including interlayer toughening in laminated composites.

The basic working principle of electrospinning was depicted in Figure 2.4:.

Electrospinning system basically consisted of the polymer solution, feeding system, high voltage power supply, and collector. When the electric field generated between the collector and syringe tip reached a critical value, polymer was jetted from the needle tip towards to the collector. Meanwhile, the solvent in the solution evaporated and the nanofiber structure was formed on the collector. According to the required properties of nanofibers, applied voltage, needle to collector distance, concentration of the polymer solution and feeding rate could be adjusted.

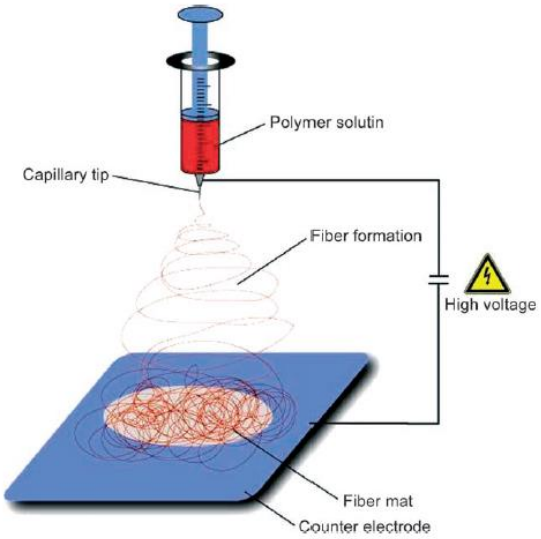

Figure 2.4: Basic electrospinning principle [20].

Apart from collectors which were used for the production of randomly oriented nanofibers, different collector assemblies (as shown in Figure 2.5**:**) were studied to obtain aligned nanofibers. As depicted in Figure 2.5**:**.a, the biggest disadvantage of the collector was the tendency of nanofibers to collect onto wire not onto the drum. Also, to adjust the length of aligned nanofiber for the parallel electrodes caused problems. The same problem occurred for Figure 2.5**:**.c, the thickness and the length of nanofiber layer was achieved at some level that limited to attain required properties [21].

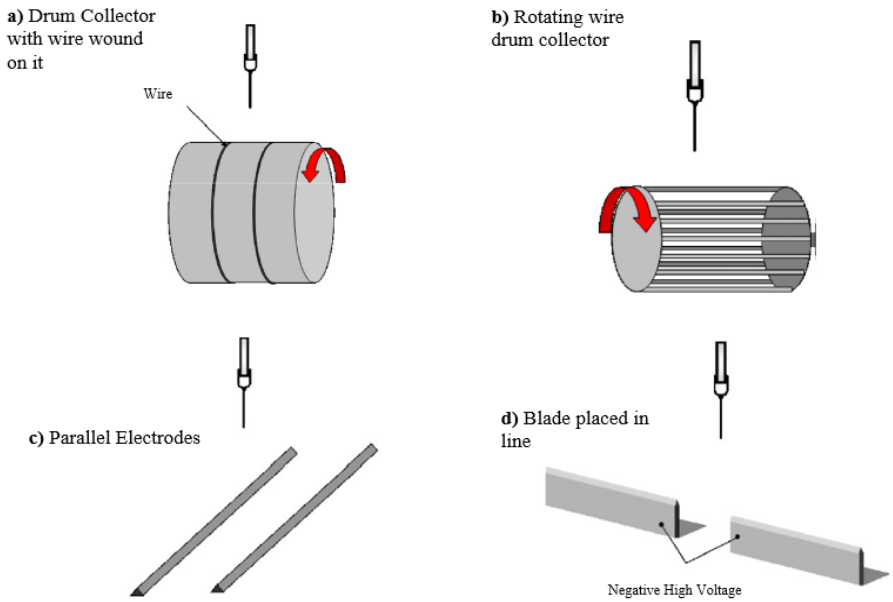

Figure 2.5: Collector assemblies for the production of aligned nanofibers.

To date, the different type of nanofibers produced by electrospinning method was investigated as an interlayer toughening element in laminated composites. By using polycarbonate nanofibers as a toughening element, Sihn et al., reported an increase in mechanical performance under loadings both in-plane and out-of-plane. Polycarbonate nanofiber interlayered carbon/epoxy composite system showed 8.5% microcrack initiation enhancement under tension loadings [22].

Zhang et al. investigated the effects of polyether ketone cardo (PEK-C) nanofiber diameter and thickness on mechanical performance and toughening characteristics in carbon fiber/epoxy composite. Interlaminar fracture toughness was enhanced by the addition of 0.4% weight loading of nanofibers in composites and it was reported that finer nanofibers resulted in better mechanical performance under flexure loadings [23]. In another study reported by Jiang et al., nylon-6 nanofiber reinforced thermoplastic polyurethane composite films were prepared and both interface morphology and the composite properties were investigated. It was emphasized that when the nanofiber thickness getting higher, wetting capability of the composite decreased. Also, significant enhancement in mechanical properties was determined with the 0.4wt% nylon-6 nanofiber presence within composite [24].

In another study which was reported by Palazzetti et al., the effect of nanofiber orientation, nanofiber thickness and nanofiber diameter on mechanical performance carbon fiber reinforced laminates as interleaves were investigated. It was concluded that when the thickness of nanofiber got higher, interface performance decreased. Also, the smaller fiber diameter led higher energy absorbing capability as an interleaf between laminates [25]. Zussman et al., investigated the PAN derived carbon nanofibers as an interlayer and bending modulus of composites was measured as 69 MPa [26]. In another report, core-shell nanofibers as PA-6 as a core, PMMA as shell were fabricated by means of the hot press method. Thermal stability of the composite increased with the nanofiber increase within composite content [27].

The brief summary of nanofiber reinforced laminated composite reports were listed in Table 2.1.

Table 2.1: Literature review which nanofibers used as toughening element.

Composite System	Material of Nanofiber Interlayer	Characterization	Results
Glass fiber/epoxy	Polycaprolactane	Double cantilever beam (DCB)	GIc initiation 20% GIc propagation 12% [28]
Carbon fiber/epoxy	Poly(e-caprolactone)	DCB	GIc initiation 37% GIc Propagation 92% [29]
Carbon fiber/epoxy	Nylon 6,6	DCB	Delamination Toughness 130% [30]
Carbon fiber/epoxy	PA66	End notch flexure (ENF) DCB	GIc 156% GIIc 69% [31]
Glass fiber/epoxy	Nylon 6,6	DCB ENF	GIc 62% GIIc 109% [32]
Carbon fiber/epoxy	P(St-co-GMA)	3 point bending (3Pb) ENF	Flexural strength 16% GIIc 55% [33]

2.4 The Role of Nanomaterials in Interface Toughening

In general, nano-scaled materials such as nanoclays, halloysite nanotubes, graphene and CNTs which were taken up to 100 nm could be used in the case of interface toughening of laminated composites.

To improve out-of-plane properties of epoxy composites, nanoclay was applied to increase matrix toughening and to create crack deflecting ones within laminates. With the proper dispersion of nanoclays in the epoxy resin, flexural modulus and strength of composite were enhanced in 15% and 40% respectively [34]. In another study which halloysite nanotubes used as a reinforcement material in the epoxy matrix. With the addition of halloysite nanotubes into epoxy, 25% increase in interlaminar shear strength and enhanced flexural strength under loadings of Mode-I and Mode-II were investigated [35].

However, particle-based reinforcements due to the dispersion problems of inclusion materials. So the agglomerated inclusions led crack spots which caused a decline in the overall performance of laminated composites.

2.4.1 CNTs as a reinforcing element in interface toughening

CNTs had been proven the strongest known material because of high mechanical, electrical and thermal properties by the time discovered by Iijima [36]. With the attracting properties of CNTs as mechanical, thermal and electrical performance, in different forms of CNTs were used in various applications as shown in Figure 2.6 Physical properties of CNTs was shown in Table 2.2.

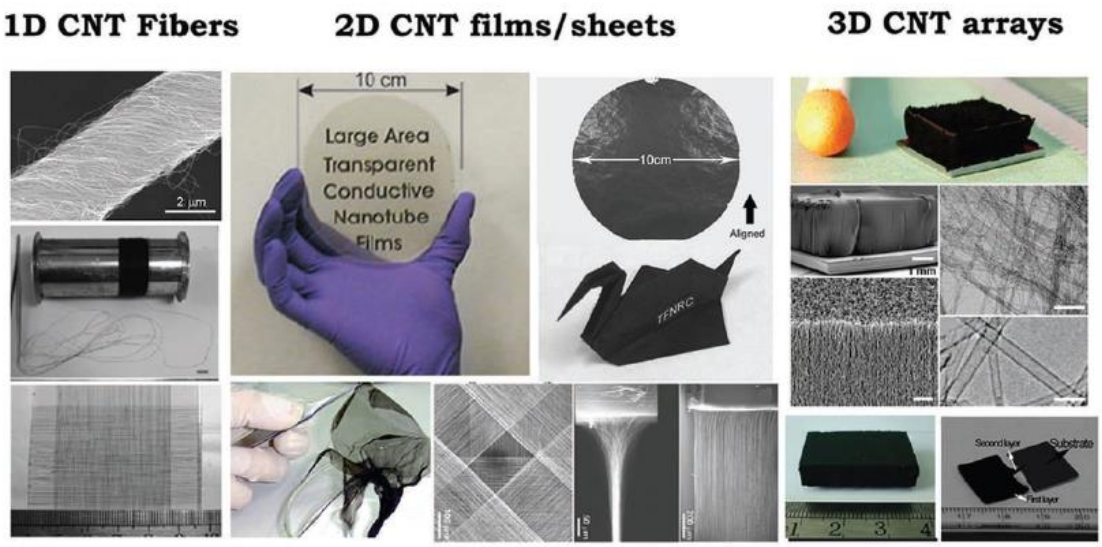

Figure 2.6: Potential applications of CNTs [37].

Table 2.2: Physical properties of CNTs.

Property	SWCNTs	MWCNTs
Density (g/cm^3)	0.8	1.8
Electrical Conductivity (S/cm)	10^2-10^6	10^3-10^5
Thermal conductivity (W/mK)	6000	2000
Thermal stability in air (˚C)	>600	>600

CNTs was a tubular structure whose graphitic layer rolls onto this structure as seamless, existing in depending on wall numbers as single wall carbon nanotubes (SWCNTs) consisting a single rolled graphite sheet and multi walled carbon nanotubes (MWCNTs) with many rolled concentric graphite sheets as shown in Figure 2.7. The properties and the structures of SWCNTs and MWCNTs differed from each other.

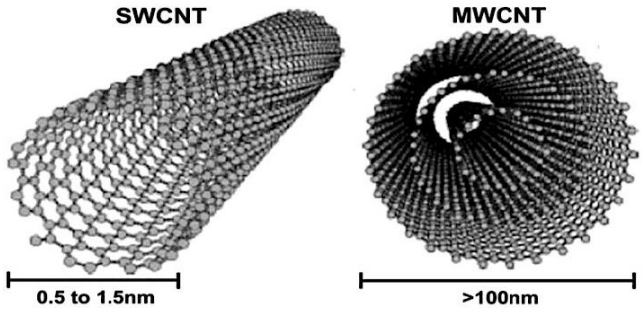

Figure 2.7: Schematic view of SWCNTs and MWCNTs [20].

The reason behind the high conductivity properties of CNTs is the state of sp^2 hybridization. With the energy excitation, carbon rised from ground state which had an electron configuration of $1s^2\ 2s^2 2p^2$ to excited state which was illustrated as $1s^2\ 2s^2\ 2p^2$. In this configuration, there were strong electrons in 1s orbital, whereas comparably four weak atoms in 2s and 2p orbitals. This was called as sp^2 hybridization which provided carbon atom to make 4 bonds.

Overall CNTs properties in structures was related to the length and diameter of CNTs. If the CNTs had a long length, entanglements in polymer matrix could be encountered. However, longer length provided low electrical percolation threshold and good mechanical performance. In the case of CNTs diameter, SWCNT provided large interfacial area and less stiffness depending on large diameter. In contrast, MWCNTs had a higher mechanical and electrical properties, also was more stiff then SWCNTs.

Since there have been numerous different methods for CNTs production, mostly used CNTs production methods were arc discharge, laser ablation and chemical vapor deposition (CVD) as depicted in Figure 2.8. These production methods which had advantages like produced CNTs structure, suitability of CNTs production conditions to industrial-scale made them important from the other methods. In arc-discharge method as depicted in Figure 2.8.a, by creating electrical arc between two graphite anode and cathode electrodes, carbon was vaporized and condensed as a nanotube. Without the presence of a catalysis, CNTs production could be conducted, but the quality of the CNTs was worse than the other production techniques. It was needed to make an extra purification step to enhance the CNTs quality. Arc discharge method firstly used by Iijima for the production of CNTs. In the case of laser ablation method which was similar to arc discharge, laser was shot to the graphite surface and formation of CNTs was generated at this graphite surface. Instead of electrical sparks, laser was

used for the generation of nanotubes. Another method which produced higher quality CNTs was CVD. In CVD system as a carbon source hydrocarbon gases such as methane, ethylene were used. The growth of CNTs started at the time of carbon source and carrier gas passed over through the tube. SWCNTs or MWCNTs could be produced by means of CVD system with the change of temperature rates [38].

CVD system was used firstly for the purpose of CNTs growth by Yacaman et al., CVD method had advantages like control over final CNTs pattern on large areas and high quality production of CNTs. CVD drew attention due to its advantages such as; controlled growth and alignment, high yield *etc*. Whereas residual particles in arc-discharge and laser ablation were carbonaceous impurities, in CVD method consisted residual catalysis particles [39].

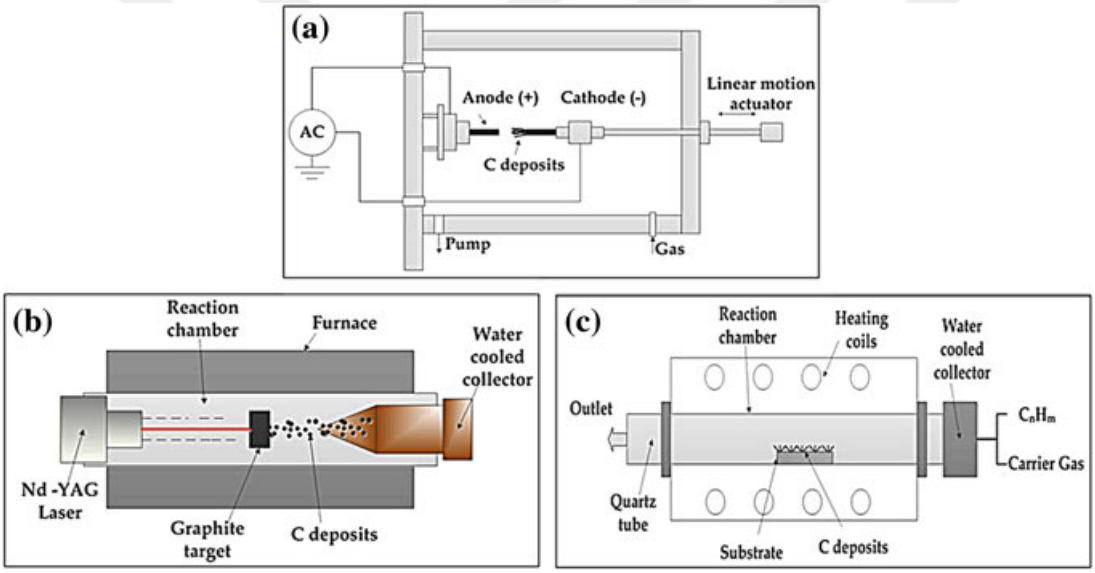

Figure 2.8: (a) Arc discharge method (b) Laser ablation technique (c) CVD [38].

The morphology and surface texture of the substrate material greatly affected the CNTs quality and yield. Especially the interaction between the catalyst and substrate changed the catalytic behavior of the catalysts during growth. To date, there were different substrates used for CNTs growth such as alumina [40], silicon [41], zeolite [42], graphite [43], sapphire [5], Al_2O_3 fiber [44], carbon fiber [45] *etc*. In a study which CNTs growth carried out on Al_2O_3 and SiO_2 substrates by using different catalysts (Fe, Co, and Fe–Co) reported that more quality MWCNT growth was succeeded on Al_2O_3 substrate with Fe–Co catalysts in comparison with SiO_2 due to the high catalyst-substrate interaction leading to better metal dispersion, non-agglomerated metals and less defective MWCNTs production [46]. The substrate

material also plays an important role in the alignment, density, and diameter of CNTs. While aligned or curly MWCNTs formations produced on the quartz substrate at 850˚C-900˚C, randomly oriented MWCNTs generated on alumina substrates at 800˚C-900˚C [43]. The reason of the randomly grown CNTs on the alumina substrate was the low Van der Waals interaction between outer walls of the nanotubes. Lee et al. studied the control of CNTs density by changing the porous structure of the substrate which changed the catalyst-substrate interaction [47]. Apart from alumina, silicon substrates, another study reported by Hongo et al., CVD process applied on the iron-coated sapphire substrate and the control over the growth of CNTs could be provided according to different crystallographic faces of the sapphire substrate [5].

Surface roughness was one of the main effects of the diffusion rate of catalyst particles on the substrate which was reported in a subject by reported by Seidel et al. Rougher surfaces obstructed diffusion of catalyst into substrate resulting larger particles onto the surface. As illustrated in Figure 2.9, SWCNT growth directly influenced by the diffusion rate of the catalyst. If the diffusion rate was high, clustering of catalysts was more expected (Figure 2.9.a) whereas strong interaction hindered requested catalyst formation (Figure 2.9.c).

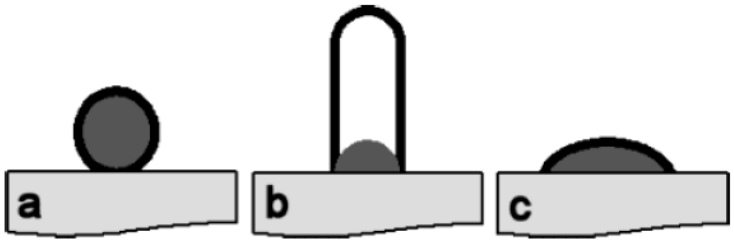

Figure 2.9: Schematic view of interaction between catalyst and substrate affecting growth of SWCNTs [48].

The interaction between substrate and catalyst could be chemically or physically which depended on various parameters such as; the catalyst dispersion on the substrate, the phase, the porosity and the surface roughness of the substrate [49]. Also, this interaction influenced the electronic structure of catalyst which greatly determined the dispersion of metal catalyst on the substrate and also, interaction played an important role in the determination of CNTs growth mechanisms as depicted in Figure 2.10.

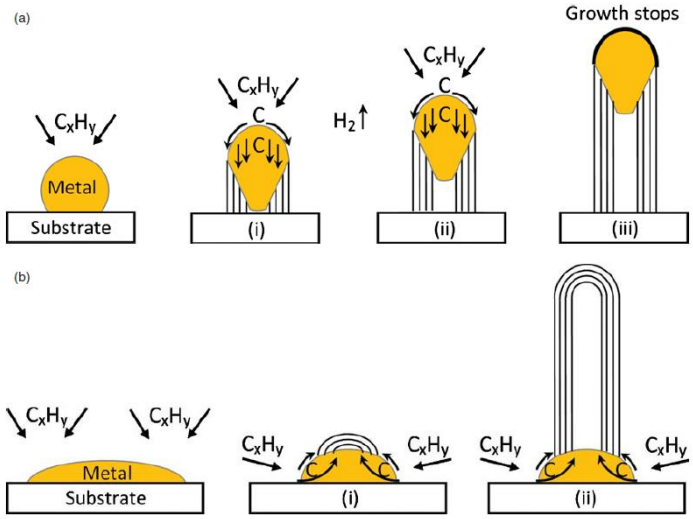

Figure 2.10: CNTs growth mechanisms: (a) tip-growth model, (b) base-growth model [50].

For the tip growth model, weak interaction between metal and substrate caused the diffusion of carbon through the metal and forcing to leave the metal particle from the substrate. But, if base growth interaction was strong so metal catalyst could not be lifted off from the substrate. CNTs could not lift the metal particle and growth occurs on the base part of the catalyst.

2.4.2 CNTs reinforced thermoplastic-based laminated composites

To date, most of the literature focused on CNTs reinforced thermoset-based laminated composites, and reports on CNTs reinforced thermoplastic-based laminated composites were relatively limited. Incorporation of CNTs into interlayer cacould be achieved with different approaches such as placement of buckypaper as an interleave, nano-stitching of CNTs, coating of fiber with CNT-containing sizes, impregnation of CNTs-resin onto fiber, nano-stitching of CNTs onto fiber, the growth of CNTs onto fiber, etc [51].

In a study which was reported by Garcia et al., aligned CNTs were used as nano-stitching elements as shown in Figure 2.11 between adjacent plies at less resin rich spots within interface. The function as a bridge of CNTs between plies increases interlaminar toughness and overall laminate performance [52].

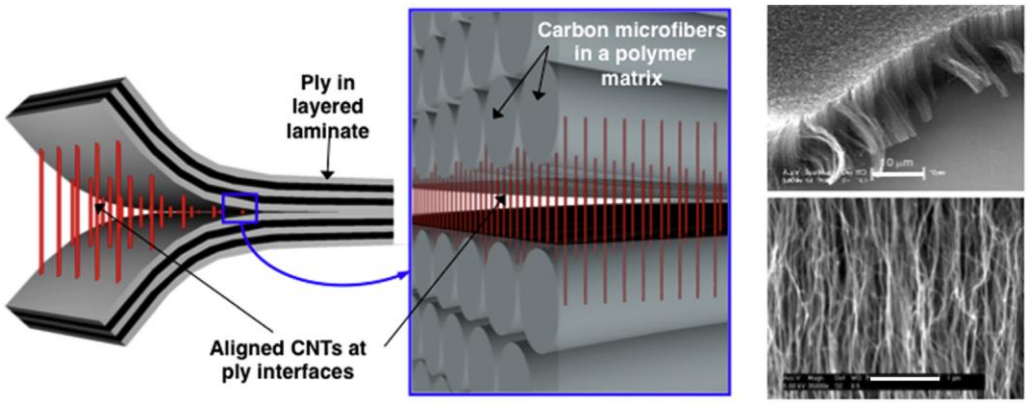

Figure 2.11: A-CNTs as nano-stitching elements onto fiber [52].

Diez-Pascual et al. reported the comparison of thermal, electrical and mechanical performances of polysulphone (PS) compatibilized poly(ether ether ketone) (PEEK)/single-wall carbon nanotubes (SWCNTs)/glass fiber (GF) laminates with non-compatibilized glass fiber laminates which all manufactured with melt-blending and hot pressing. The increase in thermal degradation was explained as the 'barrier effect' of SWCNTs which hinders the degradation diffusion. Also, PS compatibilizer provides SWCNTs easily incorporate with the matrix and provides SWCNTs to show its 'barrier effect' property efficiently [53]. Shen et al. followed the same route and discussed mechanical and thermal properties of prepared CNTs-reinforced polyamide-6 (PA6)/GF laminated composite. CNTs/PA6 nanocomposite shows 17% and 18% enhancement in tensile modulus and tensile strength respectively when compared with the neat PA6 laminated composite and also up to 2 wt% CNTs incorporation increased flexural stress of laminates 36%. However, when the CNTs concentration gets higher than 4 wt%, mechanical performance of laminates cannot increase due to the poor wetting and adhesion occur between the laminates because of the high viscosity [54]. Apart from melt-blending of CNTs, incorporation can be performed with the dispersion of CNTs in fiber sizing which provides a stress transfer at the interface region. Rausch and Mader focused on the tailoring of interphase sensors constituting CNTs for the application of health monitoring. Multi-wall carbon nanotubes (MWCNTs) coated GFs embedded into polypropylene (PP) matrix was prepared and their electrical conductivity at the interface was investigated. It was reported that 0.09% MWCNTs addition to the sizing provides better conductivity results in comparison with the melt-blended MWCNTs/PP composite due to the improved dispersion of CNTs [55, 56]. Besides mentioned incorporation methods of CNTs into polymer/fibers, the growth of CNTs onto fiber was mostly preferred due to having the

feasibility of high loading CNTs addition. In a study reported that an enhancement in interfacial shear strength (IFSS) of CNTs grown carbon fibers onto poly (methyl methacrylate) (PMMA) matrix was about 26% which is attributed to the improved stress transfer between carbon fiber (CF) and the polymer matrix. Also, good wettability of grown CNTs with PMMA polymer was reported with drop-on-fiber method [57]. Rahmanian et al. synthesized MWCNTs onto CFs and GFs via chemical vapor deposition method (CVD) and CNTs coated fibers were embedded into PP matrix. The reason behind the 40% and 39.2% improvement in tensile (E) and flexural modulus (E_f) for randomly grown MWCNTs onto GFs composite compared to neat PP/GFs composite was explained as an effective coupling and load transfer between fiber and matrix which was generated by MWCNTs. Also, 57% and 51% increase in E and E_f were reported for the MWCNTs coated CFs over neat CFs/PP composite [58]. In the case of toughening with fuzzy fiber as an interface element, Veedu et al., investigated the fracture toughness by preparing 3D composites by using aligned CNTs onto SiC fiber. 348% and 54% enhancement in Mode I and Mode II were reported [59]. Garcia et al. prepared direct aligned CNTs into a woven fabric as depicted in Figure 2.12 and effect of CNTs alignment in laminated composites was reported. 69% enhancement in interlaminar shear strength, 10^8 enhancement in electrical conductivity through thickness was investigated.

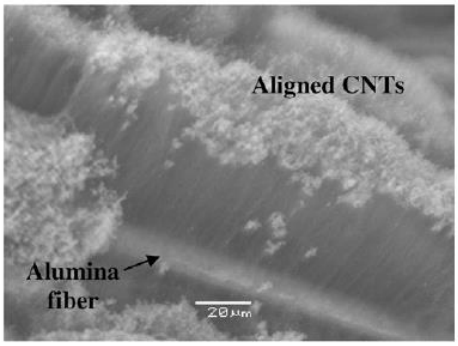

Figure 2.12: Aligned CNTs onto alumina fiber [52].

Aligned morphology of CNTs was reported by Qian et al., to be the main reason resulting in an increased interlaminar fracture toughness and electrical conductivity. Also producing CNTs onto fiber surface enabled mechanical interlocking while increasing surface area Alignment control and high volume fraction CNTs could be obtainable with the way of direct growth of CNTs onto fiber. Aligned CNTs offered lots of advantages like same tube diameter within the structure, the homogenous

orientation of tubes and higher purity when compared with the randomly oriented CNTs. So, aligned CNTs in polymer composites provided higher load transfer and mechanical interlocking between polymer and CNTs which resulted better interface toughening [51]. When compared with the other nanomaterials like SiC whickers or other nanoparticles grown onto fiber for the purpose of enhancement in the fiber/matrix interface, CNTs possessed better alignment control, low density, high surface area and better mechanical properties. Interfacial shear strength was the most important factor to efficiently ensure load transfer between CNTs and matrix to be benefited from properties which CNTs possessed in interface toughening. Mechanisms of load transfer between fiber and matrix could be explained as micromechanical interlocking, chemical bonding and Van der Waals bonding between structures [60].

In another route for interface toughening, Khan and Kim showed a 31% and 104% increase in interlaminar shear strength and Mode-II fracture toughness respectively with the incorporation of bucky paper which was made from carbon nanofibers in carbon fiber reinforced polymer composites. A strength enhance was collaborated with toughening in the crack-bridging effect of bucky paper [61].

2.5 High Performance Polymers with Potential Use in Thermoplastic Composites

PBI polymer had the potential use in different application areas such as; high-temperature fuel cell membranes, fire-resistant materials for aeronautical applications, protective clothing and gas filtration systems, *etc*. due to its heat resistance, high strength and high thermal and oxidative stability.

PBI polymer was a long chained aromatic polymer that provides polymer high chemical and thermal stability as depicted in Figure 2.13. PBI had a high degradation temperature (750˚C) and glass transition temperature (427˚C). Because of high water absorption characteristics (15%-18% absorbed water), PBI polymer generally used in blend forms such as PBI/PI, PBI/HMA, PBI/PSF *etc*. [62].

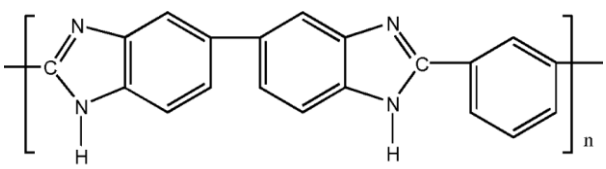

Figure 2.13: Chemical structure of PBI polymer.

For the first time Kim et al., by using electrospinning process for the production of PBI nanofiber with 300 nm diameter which showed high tensile strength [63] Weber et al. stated that PBI nanofiber produced by electrospinning process integrated into the system of electrolyte membrane fuel cell for the first time [64] Lai et al. investigated the ultra-thin PBI membranes by electron beam irradiation method and reported that cross-linked membranes showed better mechanical properties when compared with the neat PBI membranes [65]. Von Graberg et al. investigated the manufacturing of silica-PBI nanocomposites for the use in high-temperature fuel-cell membranes by means of electrospinning as shown in Figure 2.14 [66].

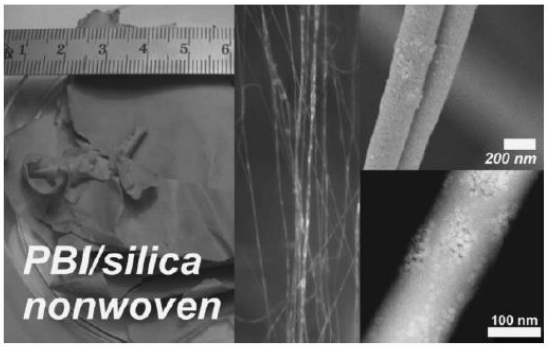

Figure 2.14: PBI-silica nonwoven.

3. MATERIALS AND METHOD

3.1 Materials

In this study, PBI S26 solution containing 26.2wt% of PBI powder with 72.3wt% N, N dimethylacetamide (DMAc) was purchased from PBI Performance Products, Inc. (USA). DMAc was supplied from Sigma Aldrich. The gel-like polymer solution, composed of 1.5wt% LiCl, was 308 g/mole, had solution viscosity of 0.46 dL/g. PBI polymer which has a chemical formula $(C_{20}H_{12}N_4)_n$ was the base polymer for nanofiber production, while DMAc was used as a solvent to dilute PBI gel. For the preparation of catalysis solution, iron (III) nitrate which had a chemical formula as $Fe(NO_3)_3 \cdot 9H_2O$ (404.0 g/molar, purchased from Emir Kimya) and iso-proponal which had a chemical formula C_3H_8O (Sigma Aldrich) were purchased. Poly (ethersulphone) (PES) which moleculer weight was 58000 g/mol in 3 mm granule size and had a linear formula, Polysulphone (PS) which has a 35000 g/mol moleculer weight and linear formula $[C_6H_4\text{-}4\text{-}C(CH_3)_2C_6H_4\text{-}4\text{-}OC_6H_4\text{-}4\text{-}SO_2C_6H_4\text{-}4\text{-}O]_n$ and Polyetherimide (PEI) which had a chemical formula $(C_{37}H_{24}O_6N_2)_n$ and granules has a size in 3 mm were purchased from Sigma Aldrich to prepare thermoplastic nanoprepregs. All chemicals were used without further purification. For the CNTs growth on commercial PBI fabric which was supplied from PBI Performance Products, Inc. and acetone were used.

3.2 Experimental Road Map of This Thesis

The road map to fabricate PBI/CNTs nanocarpets and their nanoprepregs were illustrated in Figure 3.1. Proposed method follows:

1. Randomly oriented or aligned PBI nanofibers was produced by electrospinning method, each nanofiber samples was characterized. (Section 3.3)
2. Randomly oriented or aligned PBI nanofibers were doped with Fe^{+3} by either immersion or dip-coating technique to create possible nucleation sites for CNTs growth. (Section 3.4)

3. CVD method was used to deposit CNTs on nanofiber surface. PBI/CNTs nanocarpets were characterized in terms of their electrical conductivity, CNTs orientation and yield in CVD process. (Section 3.5)
4. PBI/CNTs nanocarpets were interleaved by thermoplastic resin to prepare thermoplastic nanoprepregs, and later mechanical performance of these nanoprepregs was studied. (Section 3.5.1)

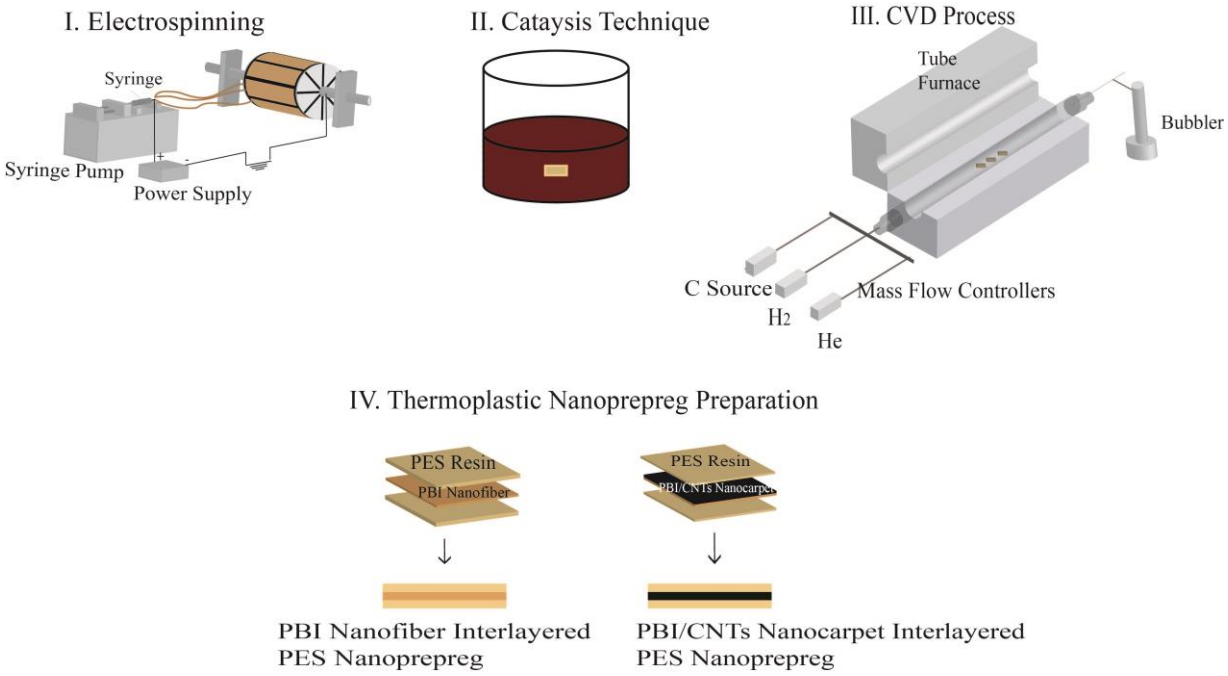

Figure 3.1: Experimental road map of this thesis.

3.3 Fabrication of PBI Nanofibers by Electrospinning

Electrospinning method was used to produce nanofibers in different orientation such as aligned and randomly oriented by using two different type of collectors as shown in Figure 3.2. Randomly oriented nanofibers firstly were explored as substrate by monitoring the quality and morphologies of CNTs. These nanofibrous substrates were catalyzed by catalysis solution at different concentration. Later on, the alignment in nanofiber production was completed by using home-built wire drum within the aim of enabling vertically aligned CNTs production onto nanofibrous substrates.

Nanofiber formation was accomplished by using electrospinning device (Argeteknolab) which consisted a pump system (NewEra NE 1000 Syringe Pump) holding the syringe (5-mL), high voltage supplier and mountable collector as rotating and home-built wire drums. The syringe needle was connected to the alligator end of

high voltage creating electrical charge. The flow rate of polymer solution was adjusted to provide stable flow profile in order to assist bead-free nanofiber formation.

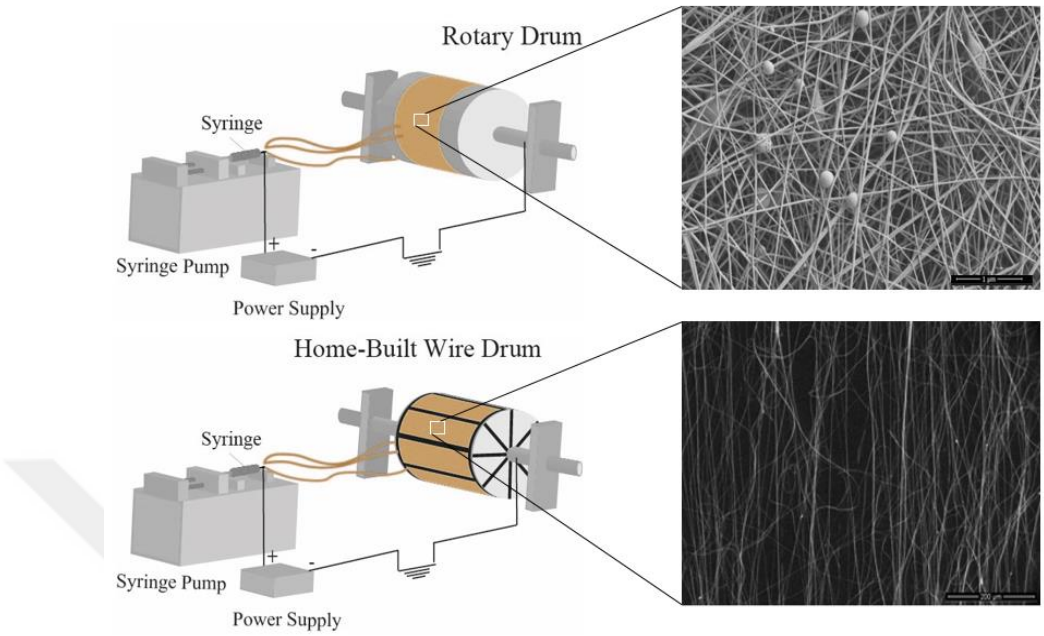

Figure 3.2: (left) Schematic of electrospinning step-up with rotate drum (top) and home-built wire drum (bottom) and (right) SEM images of randomly oriented (top) and aligned PBI nanofibers (bottom).

Nanofiber alignment was critical both to tune CNTs orientation and control resin impregnation, which long molecular chains of thermoplastic resin have difficulties to impregnate into the entangled PBI/CNTs structure. Hence, to investigate the effect of nanofiber orientation on CNTs alignment, electrospun nanofibrous mats were fabricated with rotary drum and home-built wire drum to obtain randomly and aligned nanofibers respectively. This step aimed to achieve reproducible and homogenous PBI nanofibrous substrate, which will be later used as main platform that provided structural integrity.

3.3.1 Randomly oriented PBI nanofiber production

The hypothesis was that nanofibrous substrate due to their high surface area and porous network would create an efficient platform to produce CNTs while not losing their structural integrity. These well blended PBI/CNTs networks would be beneficial as interleaves with enhanced 3D stress distribution ability and without bringing additional weight into the system. In this aim, in order to produce nanofibrous mats which could carry their own weight and be used as standing alone substrate, there different 15wt%, 20wt% and 22wt% polymer concentrations were prepared at room

temperature. First, PBI solution was dissolved in DMAc at concentration of 15wt%, 20wt% and 22wt% and stirred magnetically for 24 hours. Later the solutions were kept at oil bath at 50°C to obtain homogeneity as shown in Figure 3.3 prior electrospinning.

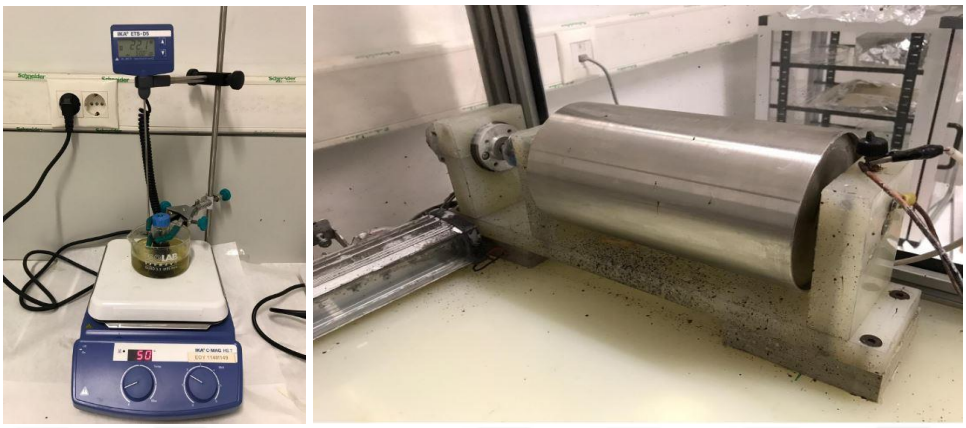

Figure 3.3: a) Polymer solution kept at oil bath b) Rotate drum mounted on Argeteknolab® electrospinning device.

Problems which were likely to occur during electrospinning process, were clogged nozzles and irregular flow of solutions. All these irregularities had significant negative impact on the quality of nanofiber production. Besides, the formation of droplets including its stability was an important factor [67]. Therefore, process parameters such as; the flow rate and voltage applied to the nozzle were adjusted precisely and these parameters for the PBI nanofiber production at concentrations of 15wt%, 20wt%, and 22wt% were listed in Table 3.1. Electrical voltage rates were arranged with increasing solution flow rates, during which the formation of polymer jet was not stable at low voltage rates. Aluminum foil was covered onto the collector, which was placed at a distance of 15 cm from the syringe needle. As listed in Table 3.1, feed rates were tuned at each PBI concentration level. So, optimum process parameters based on morphology of PBI nanofibers were determined.

Table 3.1: Electrospinning process parameters for the production of randomly oriented nanofibers.

Polymer Concentration (%wt)	Tip to collector distance (cm)	Voltage (kV)	Feed Rate (µl/hr)
15%	15	15	100
20%	15	20	150
22%	15	20	300

3.3.2 Aligned PBI nanofiber production using home-built wire drum

CNTs orientation was dependent on the distribution of catalyst particles. Hence, the orientation of PBI, the degree of entanglement and the number of intersections could local accumulation of catalyst particles. In order to avoid this problem, aligned PBI nanofibers were produced by custom-made wire drum set-up as collector. First, the wire drum setup was manufactured by using plexiglass as drum support and copper wires as collecting sites. Each disk had cut notches for proper winding of copper wire around the disks. Two disks were mounted on a wood rod 20 cm, which were placed apart from each other. The home-built wire drum was grounded and connected to step motor, and rotated at a rate of 9V. For the production of aligned PBI nanofibers, wire drum mounted on electrospinning device was displayed in Figure 3.4. Same electrospinning parameters were used to aligned PBI nanofibers at concentration of 20wt. To assure the optimum thickness, collection time of formed nanofiber was set as 2 hours, which provided both certain degree of alignment and good handling for further processes. When the collection time increased, random orientation of nanofibers were observed and alignment degree substantially decreased.

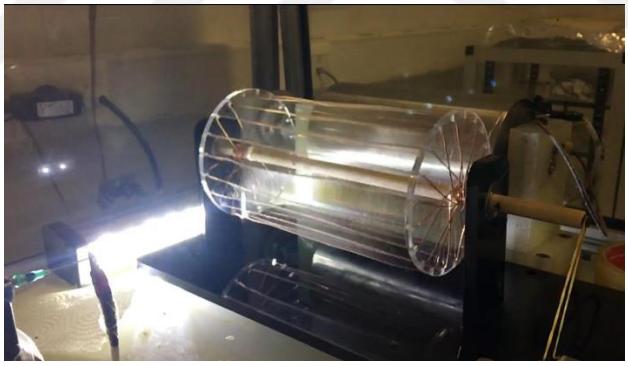

Figure 3.4: Electrospinning setup with mounted home-built wire drum.

These aligned nanofibers was used as reference interleaves and as well as substrates to produce PBI/CNTs nanocarpets. To determine the specific strength of randomly oriented and aligned nanofibers, specimen sizes were prepared as 6 cm x 2 cm and test speed was determined as 6 mm/min.

3.4 Doping of Fe^{+3} Catalysis onto Nanofibers

Metal nanoparticles were deposited on the substrate surface to act as nucleation sites Among many metallic nanoparticles, transition metals, in particular, cobalt, nickel and iron were used as catalysts for the production of CNTs. The main idea of using

transition metals was to create nucleation sites where decomposed hydrocarbon gases were deposited onto during CNTs growth process. However, iron as in the bulk form can not act as reaction initiators and assist decomposition of hydrocarbon molecules. Hence, Fe^{+3} reaction sites should be deposited in a controlled manner to trigger CNTs growth [50]. In this thesis, the coating of transition metals onto nanofiber surface was conducted by two different techniques such as immersion and dip-coating, which caused different distribution and fraction of nucleation sites. Catalysis solution contains iron(III) nitrate (having a chemical formula $Fe(NO_3)_3 \cdot 9H_2O$) and iso-proponal alcohol (C_3H_8O) at different molar ratios. The iron nitrate solution provided Fe^{+3} nanoparticles deposited onto nanofiber which accelarated the carbon solubility during the growth of CNTs. Two different solution concentration as of 50 mM and 80 mM $Fe(NO_3)_3 \cdot 9H_2O$ were prepared. In order to prepare 50 mM catalysis solution, 4.04g $Fe(NO_3)_3 \cdot 9H_2O$ was dissolved in 200 ml isopropyl alcohol, where for 80 mM catalysis solution 6.44g $Fe(NO_3)_3 \cdot 9H_2O$ was dissolved in 220 ml isopropyl alcohol. Immersion (as shown in Figure 3.5) and dip-coating technique (as shown in Figure 3.6) were both used to deposit Fe^{+3} particles on nanofiber surfaces. For the further characterizations, middle region of mats were used by trimming edges, where Fe^{+3} catalysts were mostly deposited at middle due to capillary forces.

3.4.1 Immersion technique for Fe^{+3} catalysis

Immersion technique started with the dissolution of catalysis precursor in a solvent and then it continued with placing support material into catalysis solution. In this case, the substrate material was PBI nanofibrous webs. Nanofiber swatches were cut and soaked into catalysis solution where deposited Fe^{+3} ions onto nanofibers were acted as catalyst for CNTs growth as shown in Figure 3.5. Fe^{+3} catalysed nanofibers were later kept at 50˚C for 9 hours in an ambient air to remove residual solvent molecules.

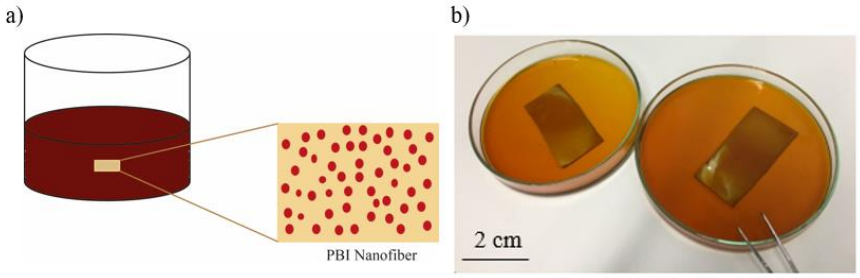

Figure 3.5: a) Schematic view of immersion technique b) Catalyst process of PBI nanofibers with immersion technique.

3.4.2 Dip-coating technique for Fe^{+3} catalysis

The dip-coating technique provided a controlled thin coating of isopropyl alcohol-based catalysis solution over nanofiber surface. In the case of dip-coating technique, 5 cycles were conducted to coat nanofibers at a rate of 200 mm/min. For each cycle, the solution was immersed in 60 seconds and dwelled at 30 seconds as shown in Figure 3.6. These catalyzed nanofibers were later kept at 50˚C for 9 hours in an ambient air to remove solvent residues. Two different molar ratios (50 mM and 80 mM) were carried out for the coating of randomly oriented and aligned nanofibers.

Figure 3.6: Dip-coating of PBI nanofiber produced at 15wt% using 50 mM catalysis concentration.

The growth of CNTs was performed on two different nanofiber substrates. The first catalysis experiments were conducted on randomly oriented PBI nanofibers. It was predicted that the CNTs grown on these randomly oriented PBI nanofibers would contribute to the network and provide an increase in mechanical performance at the interface. Second, aligned PBI nanofibers were doped with Fe^{+3} particles to have better degree of CNTs orientation coupled with enhanced electrical conductivity.

Figure 3.7: a) Coating of randomly oriented PBI nanofibers produced at 15wt% using 50 mM catalysis solution.

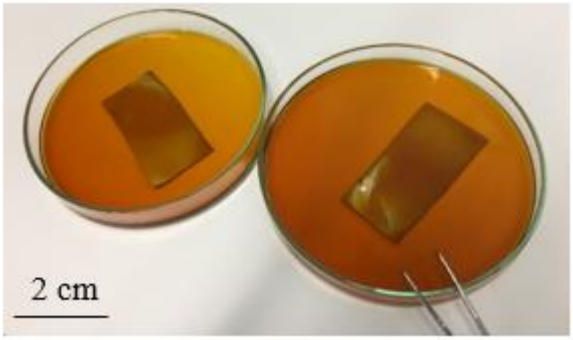

Figure 3.8: Randomly oriented PBI nanofiber produced at 15wt% immersed into 50 mM catalysis solution.

As curiosity, the CNTs growth onto commercial PBI/aramid fabrics was also explored to address the contribution of tunable PBI nanofibrous substrates. The commercially available fabric made 59% P-aramid / 40% PBI / 1% antistatic was cut as 2 cm x 6 cm and washed with acetone, and waited 6 hours to remove sizing or finishing on fabric as shown in Figure 3.9.a. It was dried at 120˚C prior the catalysis technique. 50 mM catalysis solution was using with immersion technique as depicted in Figure 3.9.b.

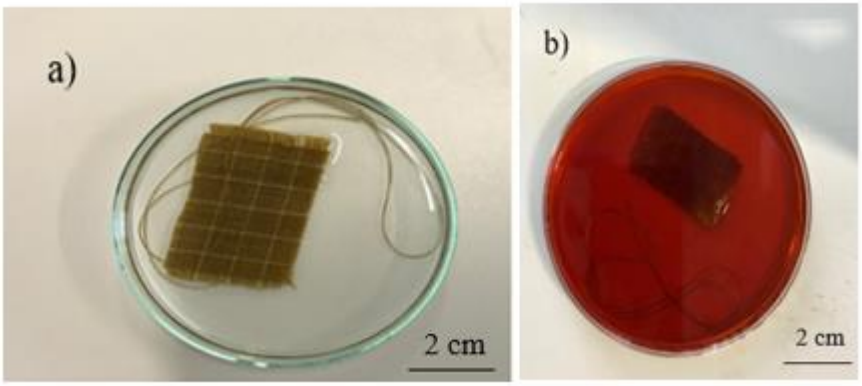

Figure 3.9: a) Commercial PBI fabric placed into acetone b) Immersion of PBI fabric in 50 mM catalysis solution.

3.5 Chemical Vapor Deposition (CVD) for CNTs Production

CVD process required a consecutive protocol to synthesize CNTs under the ambient of different gases which were used for carbon source, nucleation of catalysis and to remove ambient gases inside the quartz tube. With the increase in temperature, catalytic decomposition of metal nanoparticles firstly occurred and it accompanied the decomposition of carbon source, and caused CNTs formation. CVD set-up used in this study to produce CNTs onto PBI nanofibers as called PBI/CNTs nanocarpets was

depicted in Figure 3.10. The system had PLC controller, heater, quartz tube and mass flow controllers.

CNTs growth process to produce PBI/CNTs nanocarpets was carried out in CVD set-up in ITUARC laboratories. The catalyzed samples were inserted into quartz tube (Linberg/Blue 3-zone furnace).

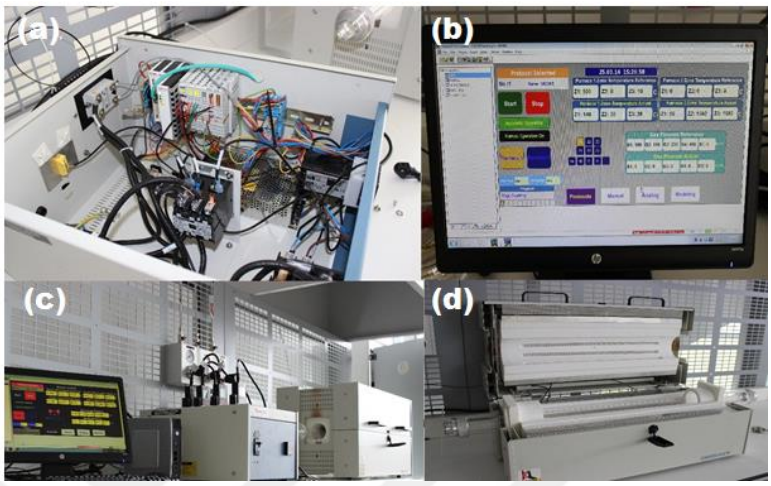

Figure 3.10: CVD system used in ITUARC exhibiting a) Heater, b) PLC, c) Mass flow controller, d) Reactor furnace.

There were five stages of CNTs growth in this approach. These were;

1. Purification (He, Ar... *etc*.): Growth process started with purging to remove all the ambient gases from the quartz tube under He gas.

2. Nucleation: Second step was the heating of the tube to promote the nucleation of catalysis particles. While heating the tube, He and H_2 gases were flown throughout the tube channel.

3. Growth: When the tube reached stable temperature, ethylene (C_2H_4) gas was inserted as a hydrocarbon source with the presence of H_2 and He.

4. Cooling: In the last step, He gas was fed while reducing furnace temperature to room temperature.

3.5.1 Fabrication of PBI/CNTs nanocarpets

3.5.2 Synthesis of CNTs onto PBI nanofibrous substrates

The growth of CNTs was processed by using modified CVD (m-CVD) method to create PBI/CNTs nanocarpets. An illustration of the CVD system was depicted in Figure 3.11. In this system, there was a tubular furnace with 2" diameter quartz tube. Gas molecules were sent through the first inlet, while gas outlet took place at the end. Under this temperature range, if catalyst had enough activation energy to overcome

barrier for carbon radical formation, CNTs production could be succeeded. In conventional vertically aligned CNTs synthesis processes, silicon wafers were preferred. In this thesis, all CNTs synthesis processes used PBI fibrous substrates. The conditioned PBI nanofibers were placed in quartz tube and the CNTS growth protocol was followed. The position of the sample inside the tube was very crucial because it changed both the distance of nanofibers to the thermocouple and the level of sent hydrocarbon. Taking into account the purity and quality of produced CNTs, samples were placed in the distance of 6-9 cm along the quartz tube.

In CVD equipment as depicted in Figure 3.11, growth protocol as mentioned in Figure 3.12 was exhibited. The system was purged first with He gas molecules at room temperature; then, H_2 was sent along with He while quartz tube was heated up to 600°C. At 600°C, H_2 was kept constant for nucleation of Fe^{+3} ions onto nanofiber sites. For CNTs growth reaction, C_2H_2 was fed as a carbon source. The total reaction time was calculated 15 minutes and then the system was cooled down to room temperature under He gas flushing.

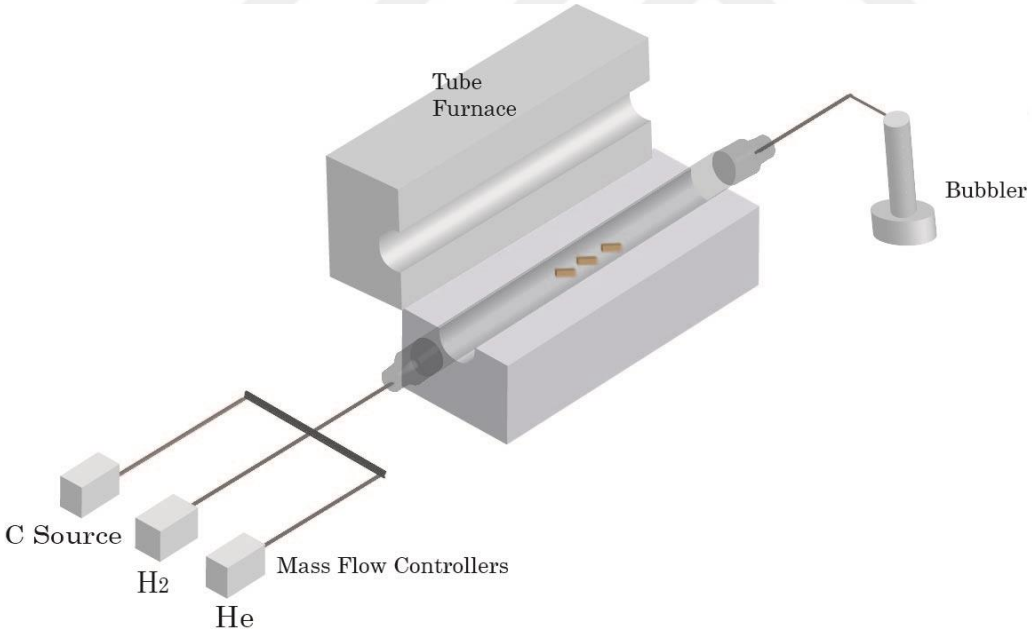

Figure 3.11: Illustration of CVD set-up.

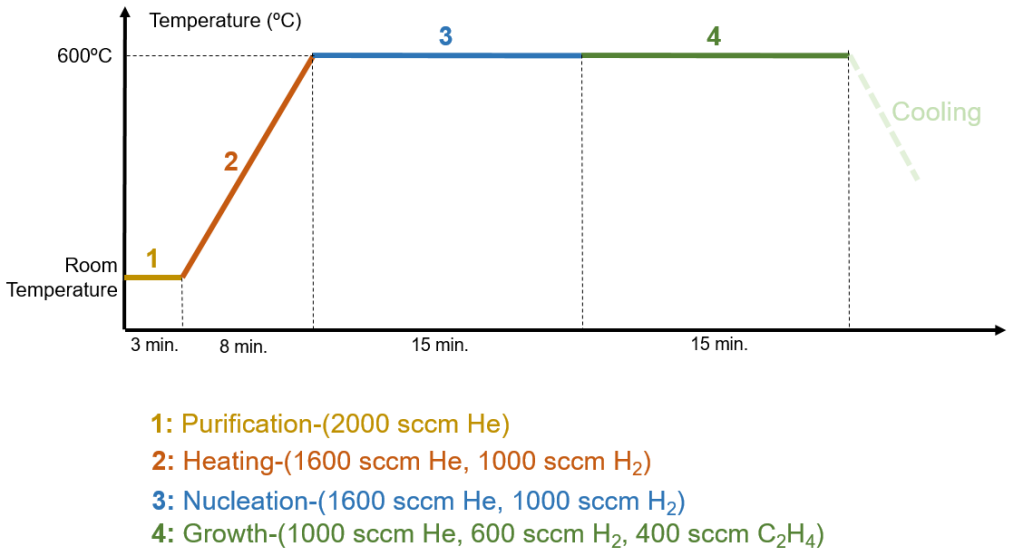

Figure 3.12: CVD growth protocol revealing time-temperature relation in each step.

3.5.3 The material selection and fabrication of thermoplastic nanoprepregs interleaved with PBI/CNTs nanoprepregs

The solubility parameters of PES, PS and PEI monomers were analyzed with Materials Studio® 8 software to predict best resin- PBI/CNTs nanoprepreg couple. Repeating unit of PBI polymer in Figure 3.13 and PES, PS and PEI monomers were displayed in Figure 3.14. Hildebrand solubility parameters were calculated for each monomers Equation 1 shows Hildebrand solubility parameter where V_m, Molar volume, ΔEv: Evaporation energy and CED: Cohesion energy density.

$$\delta = \left(\frac{\Delta E_v}{V_m}\right)^{1/2} = (CED)^{1/2} \qquad \text{Eq.1}$$

Solubility parameter pointed out the compatiblity of each polymer system. According to solubility parameters as shown in Table 3.2, it was noted that PBI and PES polymers show better compatibility than PBI-PS and PBI-PEI material systems.

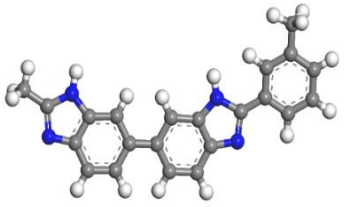

Figure 3.13: PBI monomer.

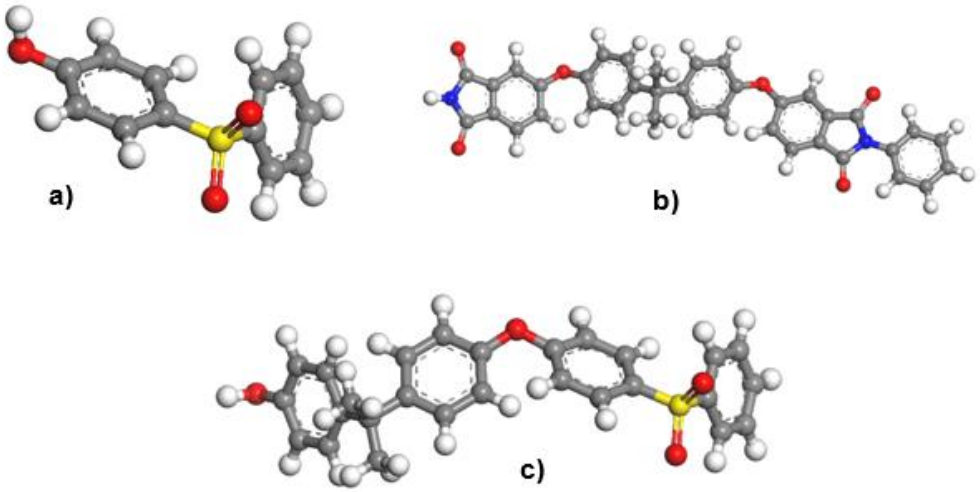

Figure 3.14: a) PES, b) PEI and c) PS Monomer.

Table 3.2: Solubility parameters of thermoplastic polymers.

System	Solubility Parameter$(J/cm^3)^{0.5}$	Solubility Parameter $(C/cm^3)^{0.5}$
PBI	22.246	10.88
PS	19.03	9.308
PES	21.591	10.561
PEI	18.575	9.085

Thermoplastic polymers could be trasferred into nanofibers in melt or solution state. PES was highly soluble in DMAc and NMP solvents. But, also PBI polymer was soluble in same solvent media which could cause dissolution of PBI nanofibers. To overcome this issue, composite preparation was performed in the melt form of thermoplastic polymers.

Thin neat PES films having 0.5 mm thickness was manufactured by hot press at 350˚ C under a pressure of 50 bar for 5 minutes as shown in Figure 3.15. Later, neat PBI nanofibers and PBI/CNTs nanocarpets were sandwiched with these PES thin films at 350 ˚C in 10 minutes at a pressure of 50 bar to produce 'PBI nanofiber interlayered PES nanoprepreg' and 'PBI/CNTs nanocarpet interlayered PES nanoprepreg' as depicted in Figure 3.16. These nanoprepregs were cooled down while placing between aluminium heads of compression moulding machine. Both PBI/CNTs nanocarpets and PES film were laid up as a laminate and then hot-pressed. Schematic view of laminate preparation was shown in Figure 3.17.

Mechanical tests were performed to determine the mechanical performance of PBI/PES and PBI/CNTs/PES nanoprepreg by following ASTM D882 standard. The speed of crossheads was determined as 0.1 times higher than the specimen thickness as stated in standard. To prevent slipping of specimens from pneumatic crossheads during crosshead traveling, top and bottom ends of specimens were epoxy coated and cured. 1 kN load cell was preferred.

Figure 3.15: Hot press used for nanoprepreg production.

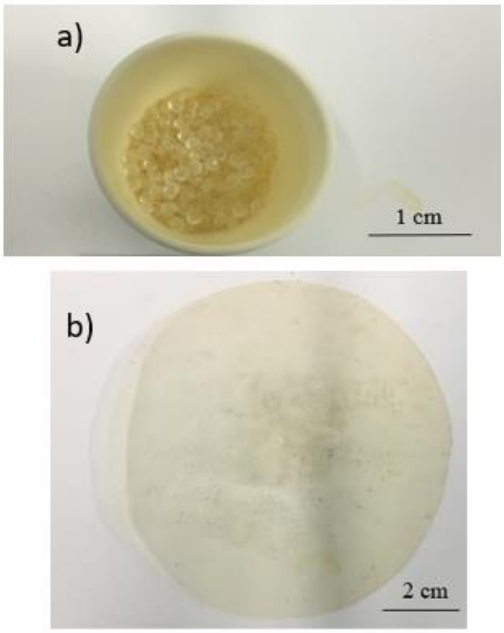

Figure 3.16: a) PES granules b) PES thin film formed by hot press.

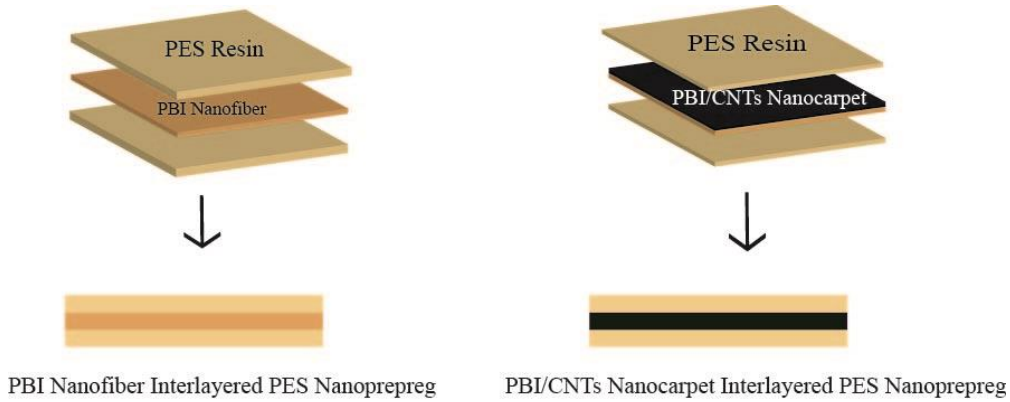

Figure 3.17: Nanoprepreg laminate stacking.

3.6 Characterization of PBI Nanofibers, PBI/CNTs Nanocarpets and Thermoplastic PBI/CNTs Nanoprepregs

3.6.1 Characterization methods used for PBI nanofibers

3.6.1.1 Morphological analysis with SEM

The main principle of scanning electron microscopy (SEM) was to scan solid surfaces with the help of high-energy electrons which are emitted from the electron source. This provided a visual information about the local structure and morphology of material [68]. Morphological analysis of PBI nanofiber was characterized by SEM which demonstrated the fiber orientation within the structure, mean fiber diameter, and surface characteristics including bead formations over the nanofiber network. The prepared samples were characterized with SEM analysis at various magnifications using with a QUANTA FEG in MEMTEK laboratory. Before characterization, samples were coated in 15 minutes with Au to hinder discharging problem during analysis.

3.6.1.2 Morphological analysis with optical microscope

Optical microscopes also called light microscopes, enable imaging using magnification ion lenses and visible light. Since optical microscopes use visible lights, magnification and resolution are limited to 500x -1000x and 0.2 mm respectively. In the case of PBI nanofibers, Olympus branded-microscope at ITUARC center was used for the determination of surface features before and after catalysis at different magnifications and resolutions.

3.6.1.3 Determination of nanofiber diameters with ImageJ

ImageJ was an important image analysis program which basically consists of image editing and analyzing. The mean nanofiber diameters were calculated with the ImageJ software. Before making analyses, images had to be calibrated according to their actual sizes. Firstly, the scale was calibrated by referencing a known length by selecting Analyze and Set Scale. Later, measurements were taken from various points of nanofibers and diameters were listed. The flow of nanofiber diameter measurement was depicted in Figure 3.18.

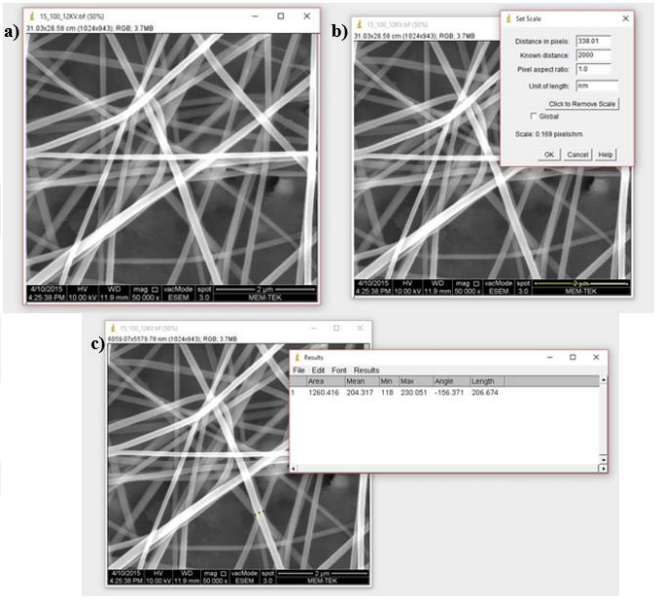

Figure 3.18: Measurement of nanofiber diameters by using ImageJ software a) Uploading image into the program, b) Defining of measurement scale-bar, c) Calculation of diameters by image processing.

3.6.1.4 Thermal gravimetric analysis (TGA)

TGA was used to characterize the thermal stability of the material by tracing the mass change occurred upon heating. The furnace of the thermogravimetric device is heated at a predetermined ramp rate changing between 0-25˚C/min. Later, the change in the temperature is monitored by a thermocouple located close to the sample. Measurements can be performed in the presence of nitrogen, and argon if it is needed to prevent oxidation of the sample [69].

To investigate the thermal stability of PBI nanofiber, test temperature was determined ranging from room temperature up to 1500˚C at a ramp rate of 10˚C/min in a nitrogen

atmosphere. TGA analyses were performed at TA Instrument SDT Q600 in SUNUM laboratory of SABANCI University.

3.6.1.5 Energy-dispersive X-ray spectroscopy mapping for distribution of catalysis particles

In Energy-dispersive X-ray spectroscopy (EDX) analysis, the electron beam is sent to the surface which breaks an electron from the surface. As the electrons from the outer orbit, while trying to pass through the orbit, the energy is released. The released energy is detected by X-rays and gives an information about the elemental structure of the specimen.

To observe the distribution of Fe^{+3} ions within PBI nanofiber after catalysis technique, elemental mapping was performed on 15wt% PBI nanofiber specimen. EDX analysis using with a QUANTA FEG was carried out in Center Laboratory of Yıldız Technical University.

3.6.2 Characterization methods used for PBI/CNTs nanocarpets

3.6.2.1 Morphological analysis of PBI/CNTs nanocarpets

SEM assisted to assess CNTs orientation, yield in CNTs growth and overall surface features. Since the diameter of individual CNTs was lower than the visible light (200-600 nm), electron microscopy is a vital technique to characterize CNTs morphology. SEM analysis at various magnifications using with a QUANTA FEG in MEMTEK laboratory was exhibited. Prior the imaging of PBI/CNTs nanocarpet, their surfaces were coated with conductive Au metal for 15 minutes.

3.6.2.2 Determination of CNTs quality with Raman Spectroscopy

Among many characterization methods used for carbon-based materials, Raman spectroscopy was one of most powerful techniques which measured the vibrational energies of molecules. This method used the inelastic scattering of a photon. The shear in the wavelength which was scattered as inelastic gave an information about the molecular structure. The positions of Raman peaks and band densities varied according to the carbon allotrope. Generally, MWCNTs exhibited two characteristic peaks as shown in Figure 3.19. D peak gave pure graphite faults at around wavelength of 1340

cm^{-1}, while G peak belonged to graphene at wavelength of 1500 cm^{-1} and 1600 cm^{-1} [70].

The density fraction of the G and D peaks were expressed as I_g/I_d, which was the ratio of sp^2-hybridized carbon amount to the degraded carbon amount. Higher I_g/I_d represented the quality and purity of CNTs.

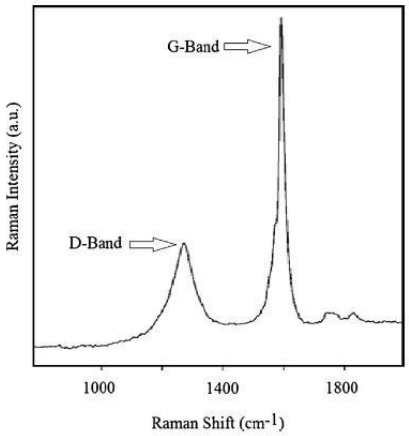

Figure 3.19: Characteristic peaks of MWCNTs [71].

Raman spectroscopy was conducted for PBI/CNTs nanocarpets using Renishaw inVia reflex microscopy with excitation energy 2.32 eV and acquisition between the ranges of 100-3000 cm^{-1}. The green laser was used for Raman analysis and all nanocarpet samples were mapped to a 40x40 micron area for the determination of D and G peaks.

3.6.2.3 Thermogravimetric analysis for PBI/CNTs nanocarpets

Both the effect of CNTs onto thermal contribution and their weight fraction into the overall structure was carried out by TGA with the temperature ranging from room temperature up to 1200˚C at a ramp rate of 10˚C/min in a nitrogen atmosphere to provide an ambient atmosphere. To discuss the CNTs' effect on thermal stability, TGA analysis was used to monitor the degradation temperatures and 1st derivatives of mass change. TGA analyses were performed at TA Instrument SDT Q600 in SUNUM laboratory of SABANCI University. CNTs grown PBI nanofibers which 50 mM catalyzed with immersion technique was subjected.

3.6.2.4 Electrical conductivity measurements

CNTs contributed to electrical conduction mechanism through individual conductive particles which was strongly influence by chirality. To determine the electrical conductivity truly depending on CNTs, measurements were conducted using 4 point

probe conductivity tester (Model FPP-470A). 4 probe point conductivity tester avoided contact problems between probes and PBI/CNTs nanocarpets or nanofibers, it provided accurate measurements. Conductivity results were calculated according to Equation.2., where σ=Electrical conductivity, d: Specimen thickness, $\frac{\Pi}{ln\,2}$=Correction coefficient. The correction coefficient was selected as 1 for thin film measurements.

$$\sigma = \frac{\Pi}{\ln 2} \cdot \frac{V}{I} \cdot d \qquad \text{Eq.2}$$

Figure 3.20: 4 point probe electrical conductivity instrument.

3.6.3 Characterization methods used for thermoplastic nanoprepregs

3.6.3.1 Mechanical performance of nanoprepregs

Tensile performance of thermoplastic nanoprepregs was investigated by pulling specimens in longitude directions until breaking occurs, in universal testing machine (UTM). Tensile strength and elongation at break values of thermoplastic nanoprepregs were reported. Tensile tests of thermoplastic nanoprepreg were carried out by following ASTM D882-12 standard in Shimadzu machine at ITU Universal Textile Center (Figure 3.21). 1kN load cell was used for tensile testing of 3 specimens per each set. (Neat PES film, PBI nanofiber interleaved PES nanoprepreg and PBI/CNTs nanocarpet interleaved PES nanoprepreg)

Figure 3.21: UTM device exhibiting tensile specimens mounted with pneumatic tensile jaws.

4. RESULTS AND DISCUSSION

4.1 Results for Neat PBI Nanofiber

4.1.1 Morphological analysis of randomly oriented and aligned PBI electrospun nanofibers

SEM micrographs and mean fiber distributions of randomly oriented PBI nanofibers at produced 15wt%, 20wt% and 22wt% were demonstrated in Figure 4.2, Figure 4.3 and Figure 4.4 respectively. Histograms were created based on at least 35 measurement by using ImageJ software. Mean fiber diameter of PBI nanofibers produced at 15%, 20% and 22% PBI concentrations were stated as 150±4 nm, 450±85 nm and 605±79 nm. It is clear that increasing PBI concentration led to coarser fibers [72], which also increased solution viscosity. Hence, electrospinning parameters including feed rate and applied voltage should be arranged to avoid any irregularities. In this thesis, as shown in Table 3.1, higher voltage was needed to enable stable flow and to avoid irregularities during feeding. Figure 4.2, Figure 4.3 and Figure 4.4 demonstrate that bead free nanofiber formation was achieved at all three different polymer concentrations. SEM micrographs also pointed out that randomly oriented nanofibers had high pore volumes which promoted interfacial adhesion of fiber to polymer matrix particularly in the preparation of laminated composites. Morphological observations revealed that that PBI nanofibers produced at 22wt% exhibited micron scale bead-like structures (as shown in Figure 4.1) while PBI nanofibers produced at 15wt% had relatively lower fiber diameters. Hence, PBI nanofibers produced at 20wt% was chosen to produce both randomly oriented and aligned PBI nanofibrous substrates.

Figure 4.1: Optical image of 22wt% PBI nanofiber.

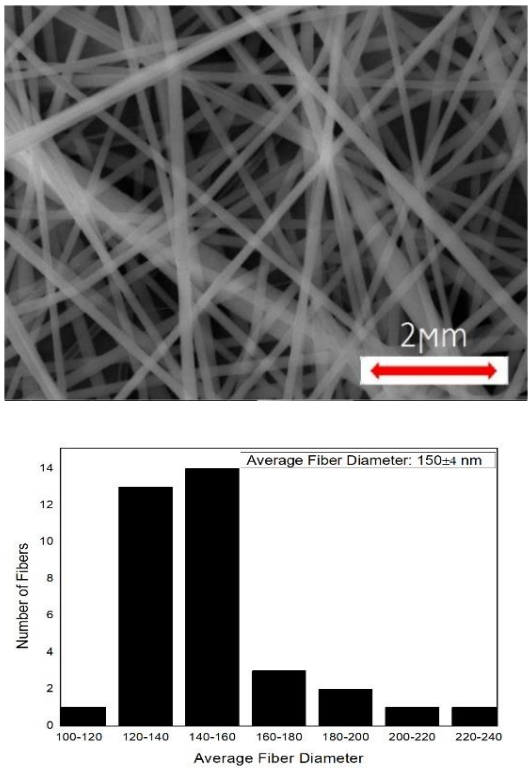

Figure 4.2: SEM image of PBI nanofibers produced at 15wt% and histogram revealing fiber diameters.

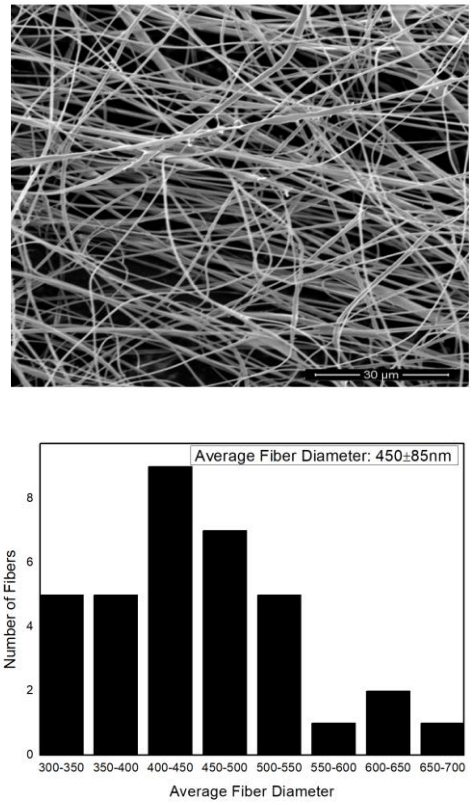

Figure 4.3: SEM image of PBI nanofibers produced at 20wt% and histogram revealing fiber diameters.

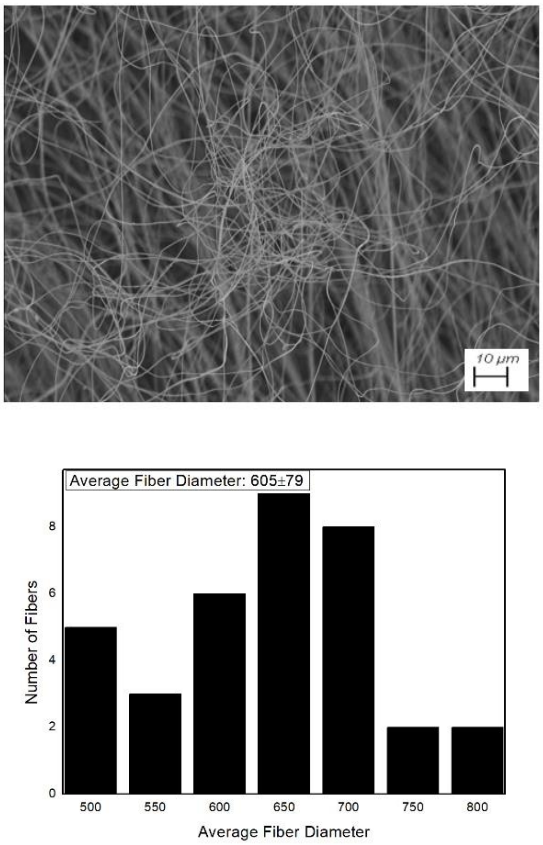

Figure 4.4: SEM image of PBI nanofibers produced at 22wt% and histogram revealing fiber diameters.

This thesis also explored the effect of fiber alignment on Fe^{+3} distribution and nucleation process. To promote CNTs orientation and benefit more from their intrinsic electrical conductivity, CNTs could be grown in a controlled fashion onto PBI nanofiber substrate.

Aligned PBI nanofiber production was achieved by using home-built wire drum and aligned morphology was partially succeeded as shown in Figure 4.5. Increasing deposition time led to inevitable randomness on the surface. In the meantime, these nanofibers should maintain their structural integrity during catalysis. Thus, partial alignment was unavoidable. Hence, 2 hours of deposition time was set. The mean diameter of aligned PBI nanofiber 20wt% was calculated as 430±42 nm.

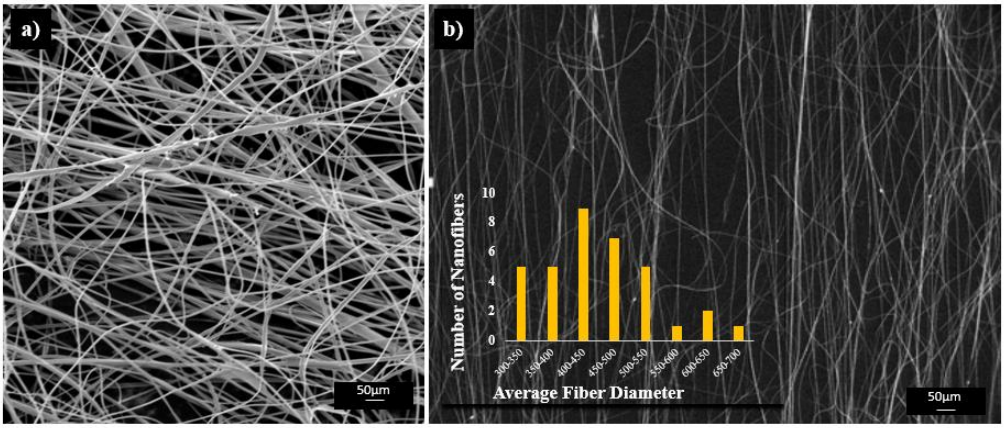

Figure 4.5: a) Randomly oriented and b) Aligned PBI nanofibers produced at 20wt% concentration.

The alignment degree of PBI nanofibers was quantified by image processing and summarized in Figure 4.6. Measurements were carried out by determining the number densities at -60˚, -30˚, 0˚, 30˚and 60˚degrees. At this point, 0˚degree was determined as vertical axis, pointing the alignment. The results showed that overall 59% alignment was achieved.

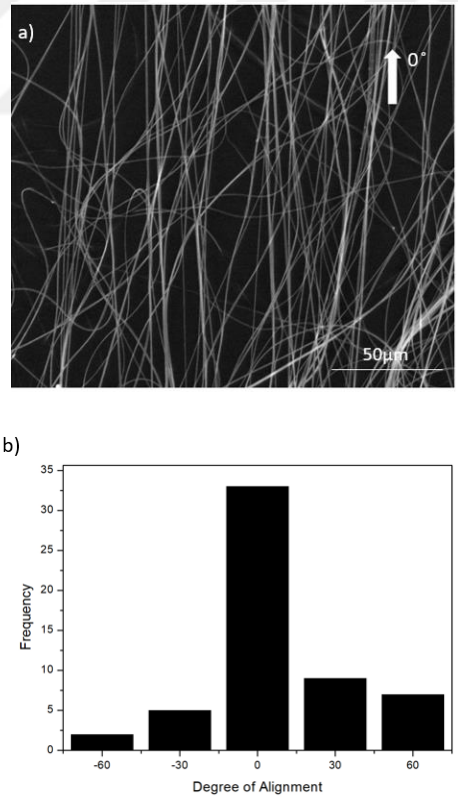

Figure 4.6: a) Aligned PBI nanofibers produced at 20wt% concentration b) The histogram revealing the degree of alignment.

4.1.2 Effect of Fe^{+3} catalysis concentration on the PBI nanofiber surface morphologies

Prior to CVD growth to synthesize CNTs, the effect of Fe^{+3} catalysis on nanofiber diameter was systematically discussed with SEM images. Figure 4.8 and Figure 4.9 show Fe^{+3} doped PBI nanofibers produced at 15wt% with catalysis solution at 5 mM and 50 mM respectively. SEM images revealed that mean fiber diameter was increased from 198±53 nm for neat PBI, to 207±53 nm for PBI nanofibers catalyzed at 50 mM and 219±52 nm for PBI nanofibers catalyzed at 5 mM. It is important to note that catalysis solution having isopropyl alcohol (C_3H_8O) and iron nitrate ($Fe(NO_3)_3 \cdot 9H_2O$) cannot dissolve PBI polymer and even had propellant interaction between isopropyl alcohol and PBI polymer. Hence, due to accumulation of Fe^{+3} particles, PBI nanofiber diameter was changed slightly after coating with the catalysis solution. Apparently, this catalysis process did not increase fiber diameter deviation.

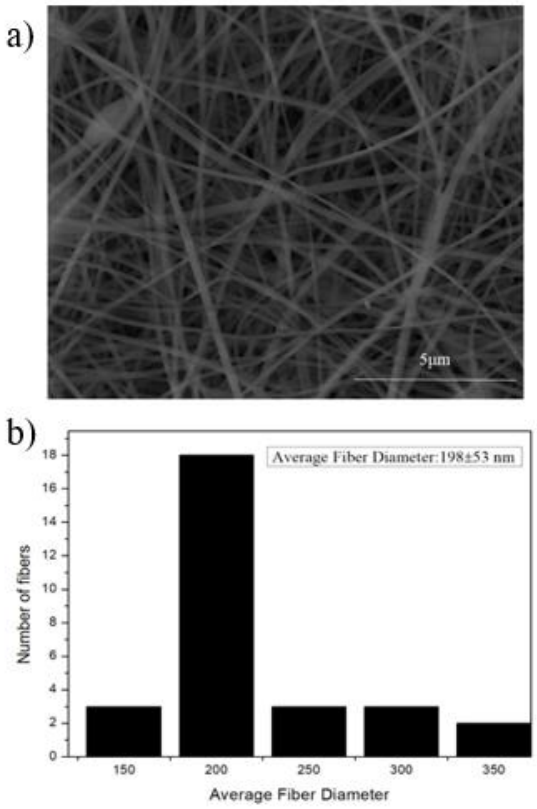

Figure 4.7: 15wt% randomly oriented PBI nanofiber morphology and its fiber diameter histogram.

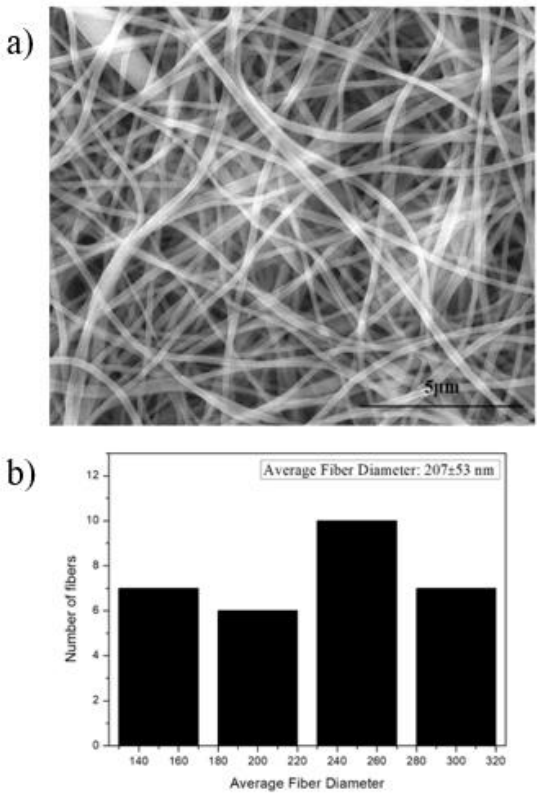

Figure 4.8: a) Fe^{+3} doped with 5 mM solution randomly oriented PBI nanofibers produced at 15wt% and b) histogram revealing fiber diameter distribution.

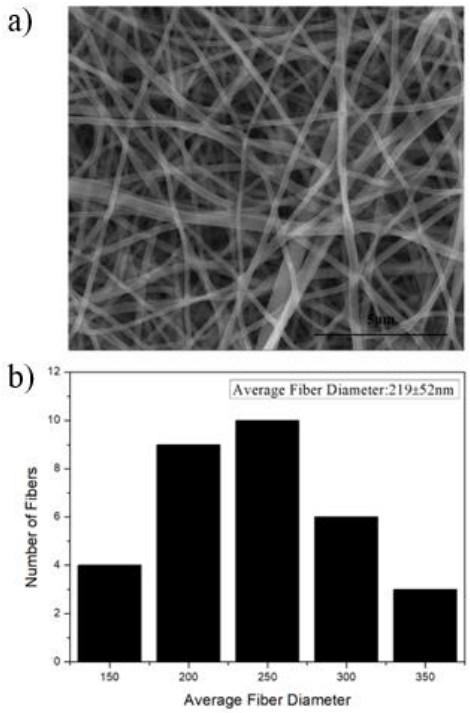

Figure 4.9: a) Fe^{+3} doped with 5 mM solution randomly oriented PBI nanofibers produced at 15wt% and b) histogram revealing fiber diameter distribution.

4.1.3 Monitoring surface morphologies of neat and Fe^{+3} doped aligned PBI nanofibers by optical microscope

We noted the increase in mean fiber diameter associated to Fe^{+3} coating in earlier section but how this process affected fiber alignment, was still intriguing. In an effort to observe the effect of Fe^{+3} doping on surface morphologies of aligned nanofibers collected at different times was analyzed in Figure 4.10 and Figure 4.11. When the collection time was longer, parallel degree of aligned nanofibers decreased and caused crimples in an entangled form [73]. The reason behind this phenomena was attributed to polymer jet oscillating in which intensity increased with longer collection time.

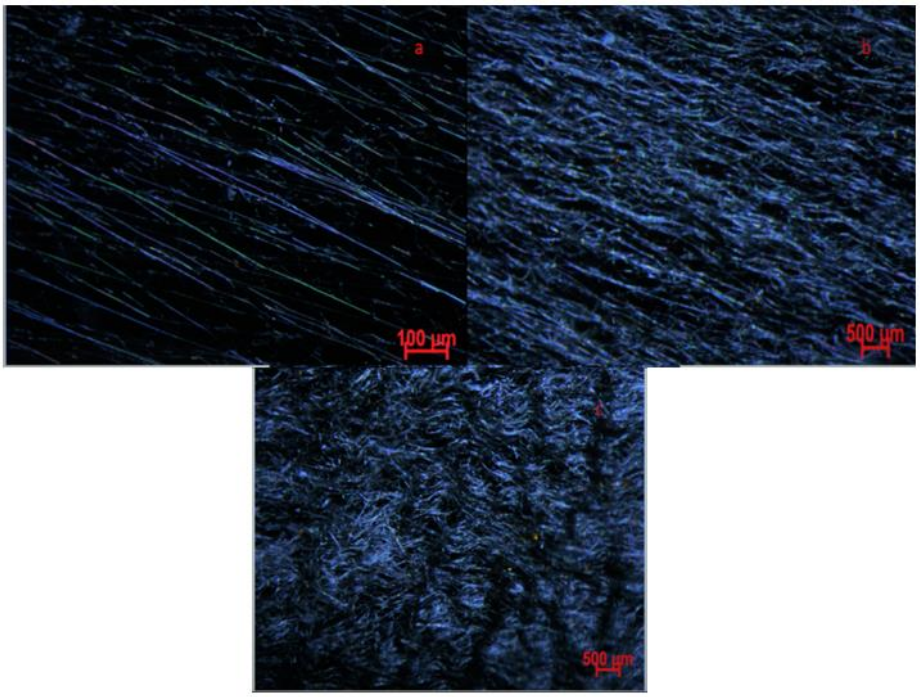

Figure 4.10: Optical microscope images of aligned PBI nanofibers at 20wt% collected at a) 1 hour b) 4 hour and c) 8 hour.

With the accumulation of catalysis particles onto nanofibers, alignment degree decreased even further as interpreted in Figure 4.10.a compared to reference Figure 4.11. Due to the wet catalysis process might cause these waviness when coupled with inevitable Fe^{+3} clusters through the nanofiber surface.

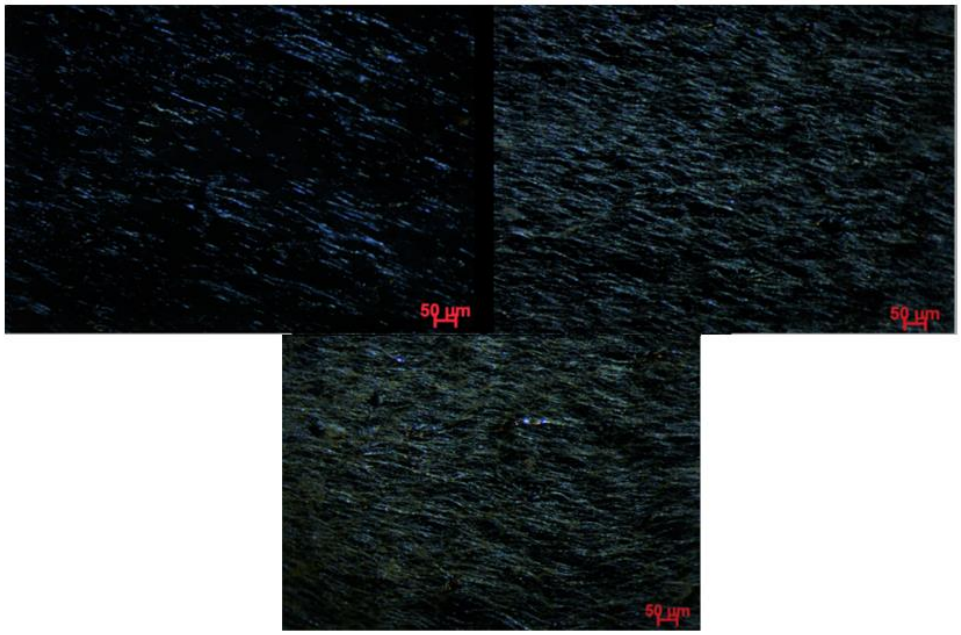

Figure 4.11: Optical microscope images of Fe^{+3} doped aligned PBI nanofibers at 20wt% collected at a) 1 hour b) 4 hour and c) 8 hour.

4.1.4 Elemental analysis on Fe^{+3} doped PBI nanofibers

This thesis also addressed the distribution of Fe^{+3} ions on PBI nanofibers where Fe^{+3} doping was not precisely controllable due to wet catalysis process. Hence, EDX analysis was performed to understand the mesoscopic distribution of Fe^{+3} ions, when the catalysis process was completed in 5 minutes. Figure 4.12 demonstrated that Fe^{+3} ion distribution was homogeneous on the fiber surface. However to detect each individual Fe^{+3} in single atomic level using SEM-EDX was not practical. Keeping in mind that these mapped points might have individual Fe^{+3} as well as Fe^{+3} clusters. Overall, it is suggested that Fe^{+3} ions were successfully accumulated on nanofiber surface to create nucleation sites.

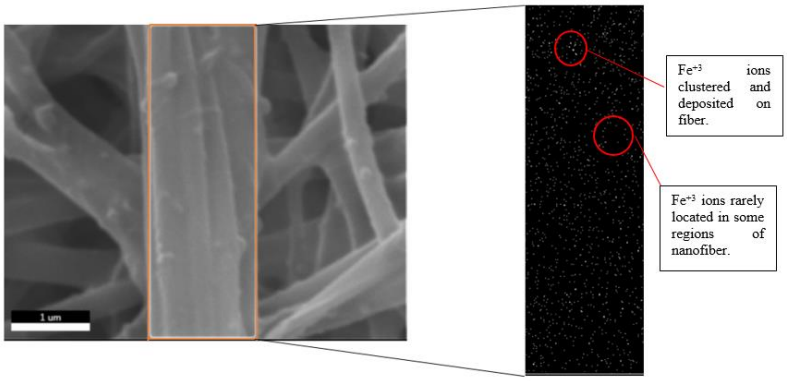

Figure 4.12: EDX analysis of 50 mM deposited onto 15wt% PBI nanofiber Fe^{+3} doped aligned PBI nanofibers at 20wt%.

4.1.5 Mechanical performance of randomly and aligned PBI nanofiber

The mechanical performance of substrates as in the form of randomly oriented and aligned PBI nanofibers was discussed in this section. The specific strength, and strain at break% of randomly oriented and aligned PBI nanofibers were reported in Table 4.1.

Table 4.1: Tensile properties of aligned and randomly oriented PBI nanofiber.

Sample	Ultimate Strength (MPa)	Elongation at break (%)
Aligned PBI Nanofiber	2.72 MPa	12%
Randomly Oriented PBI Nanofiber	13.6 MPa	15%

4.1.6 Thermal degradation of PBI nanofibers

PBI polymers do not have melting point but degraded beyond [74]. Prior CVD process, their degradation steps were revealed by TGA analysis. As displayed in Figure 4.13, the first mass change in the sample was observed at 85˚C due to the degradation of the LiCl stabilizer which was existed in polymer batch. Later, second critical mass change around at 150˚C was detected due to the evaporation of DMAc molecules entrapped in PBI nanofiber. It was observed PBI nanofibers decomposed at ca. 750˚C. Thus, CVD protocol was deliberately delivered by keeping mind on this degradation temperature not to lose structural integrity of fibers.

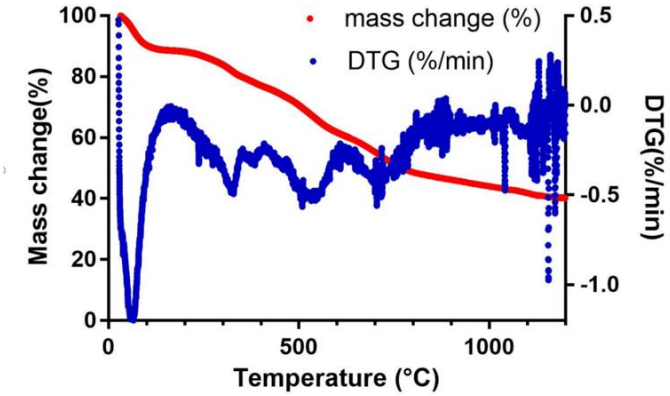

Figure 4.13: TGA analysis of neat PBI nanofiber produced at 15wt%.

4.2 Characterization on PBI/CNTs Nanocarpets

This section began with the Raman characterizations of PBI/CNTs nanocarpets, revealed morphologies and orientation of CNTs and their electrical conductivities by discussing the effect of CNTs orientation.

4.2.1 Raman analysis of CNTs quality for PBI/CNTs nanocarpets

CNTs with high purity were capable of providing better enhancement in load transfer mechanisms for interlaminar toughening and also electrical conduction mechanism. CNTs quality of PBI/CNTs nanocarpets were characterized by Raman spectroscopy.

G peak is the result of the in-plane vibrations of sp^2 bonded atoms whereas D peak is the result of the out of plane vibrations of sp^3 bonded atoms expressing the structural defects of carbon atoms. The higher value of D peak meant higher intensity of defects and more broken sp^2 bonded atoms [71]. So, the I_g/I_d ratio could be used as a measure of a graphitic structure of carbon and to quantify the structural quality of CNTs. When I_g/I_d ratios were examined in Table 4.2 for CNTs grown randomly oriented nanofibers, it was deduced that no significant difference in terms of CNTs' quality. Thus, there was not any strong correlation observed between the quality and catalyst concentration or catalysis method. Best results were noted in the case of CNTs synthesized on randomly oriented PBI nanofibers produced at 15wt% and doped with 50 mM and randomly oriented PBI nanofibers produced at 22wt% and doped with 80 mM. Apparently, I_g/I_d values were averaged out and it was not precise enough to flag dominant parameters.

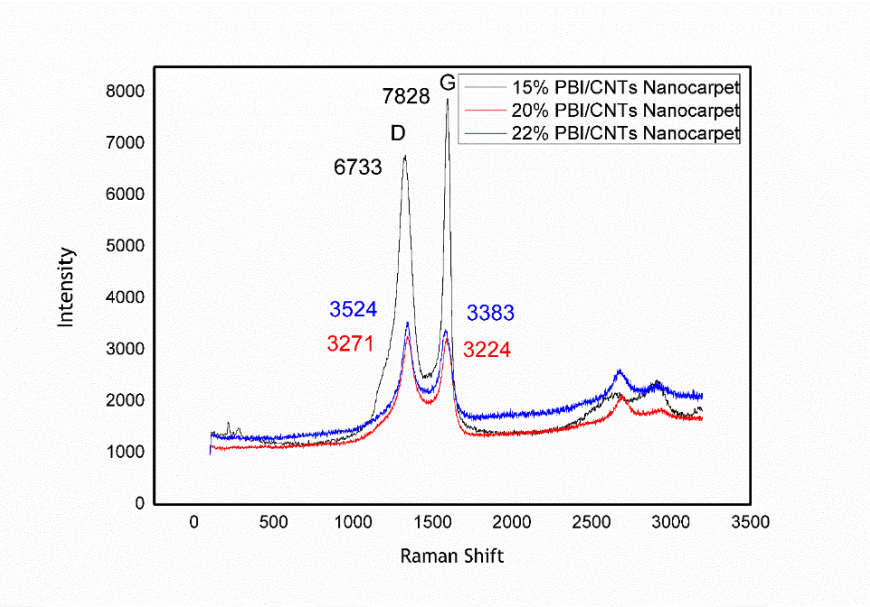

Figure 4.14: Raman analysis of CNTs growth on 15wt%, 20wt% and 22wt% PBI nanofiber immersed in 50 mM catalysis solution.

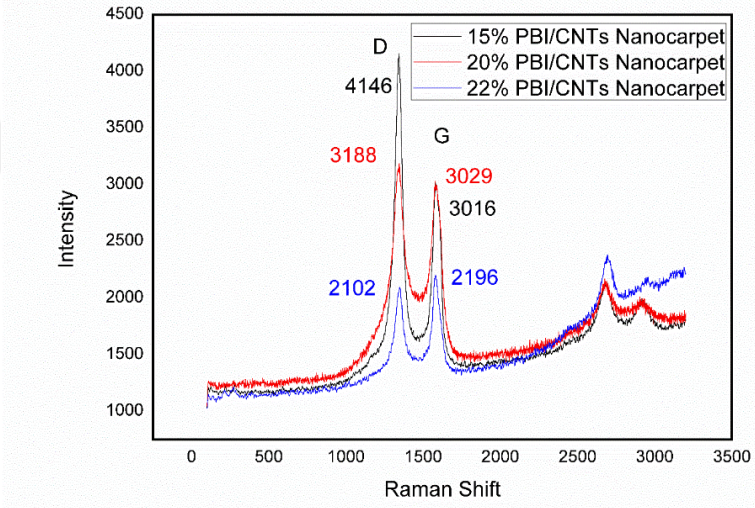

Figure 4.15: Raman analysis of CNTs growth on 15wt%, 20wt% and 22wt% PBI nanofiber immersed in 80 mM catalysis solution.

Tablo 4.1: Ig/Id ratios of PBI/CNTs nanocarpets.

Wt% PBI nanofiber	50 mM Immersion	50 mM Dip-Coating	80 mM Immersion	80 mM Dip Coating
15%	1.16	0.72	0.93	0.95
20%	0.96	0.95	1.03	0.96
22%	0.98	1.04	1.05	1.02

4.2.2 Thermal degradation of PBI/CNTs nanocarpets

PBI/CNTs nanocarpets with high thermal stability at elevated temperatures would also behave as an effective interlayer element in laminating composites. Besides, referring to neat PBI nanofibers, CNTs weight fraction could be predicted by TGA analysis. Thermal degradation of PBI/CNTs nanocarpets were determined with TGA analysis as shown in Figure 4.16. As the thermal degradation temperature of neat PBI nanofiber was determined as 750˚C from Figure 4.13, the onset of the derivative revealed CNTs degradation at c.a 900˚C. As shown in Figure 4.16, there were three significant mass change coupled with PBI and CNTs. The first weight loss was attributed to the aromatic derivatives decomposition within PBI [75] which provided stabilization, whereas the second peak was observed due to carbonization. The third sharp peak was associated with the thermal degradation of PBI polymer since it had strong intermolecular forces which provided stability at high temperatures. Overall, the results suggested that the presence of CNTs onto nanofiber enhanced the thermal stability of nanofibrous network.

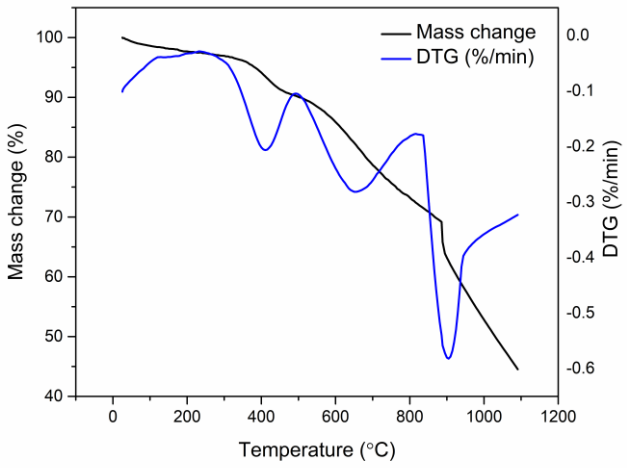

Figure 4.16: Thermogravimetric analysis for PBI/CNTs nanocarpets.

4.2.3 Morphological analysis for PBI/CNTs nanocarpets with SEM

The morphology of CNTs was influenced by different parameters such as; catalyst concentration, hydrogen and carbon treatment times, growth temperature *etc* [50]. SEM micrographs of PBI/CNTs nanocarpets grown onto randomly and aligned nanofibers were shown in Figure 4.17.a and Figure 4.17.b. Both aligned and randomly oriented neat PBI nanofiber diameters were measured as 450±85 nm and 465±50 nm,

respectively. It was clearly seen that CNTs growth temperature as of 600˚C enabled CNTs growth on PBI nanofiber either in the form of randomly and aligned orientation. More importantly, it did not cause any fiber degredation, hence it kept its structural integrity, which strongly affect handling for further steps.

To provide better mechanical and electrical performance from PBI/CNTs nanocarpets as an interlayer in laminated composites, efficient load transfer mechanism and coherent PBI-CNTs network were required. This proper interaction increased interfacial shear strength which resulted in high load transfers between the polymer matrix and reinforcement [76]. SEM micrographs revealed that the interaction between CNTs and PBI benefiting from Van der Waals forces asssisted good CNTs coverage over PBI nanofiber surface. However, CNTs orientation and CNTs length/diameter could be tuned by the changes in CVD protocol.

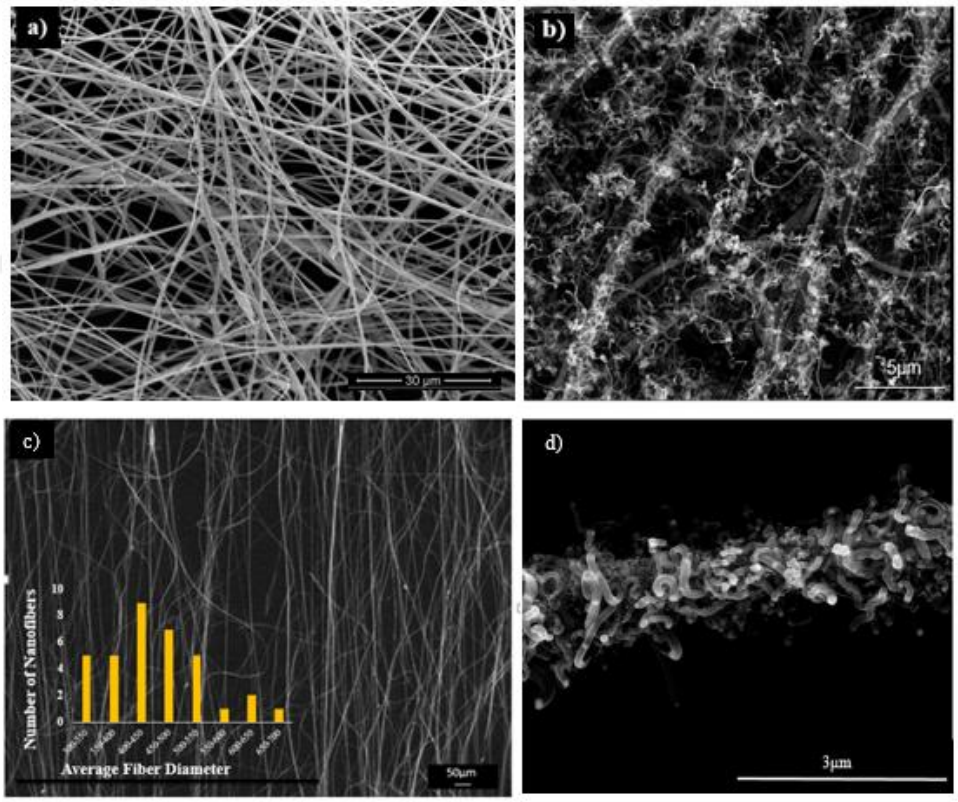

Figure 4.17: a) Randomly oriented PBI nanofiber b) CNTs grown on aligned PBI nanofiber c) Aligned PBI nanofiber d) CNTs growth on a single aligned PBI nanofiber as a zoomed view.

Physical properties of CNTs was affected by the change in the growth protocol such as growth time, nucleation time of catalysis, sample position within the quartz tube, *etc* [77]. To analyze these effects, hydrocarbon purge time and nucleation time were

changed systematically and the changes in morphologies were monitored. First, a parametric study by changing hydrocarbon purge time of 5, 8 and 15 minutes. Besides the change in purge time of carbon source, all the other variables in CNTs growth protocol remained constant as shown in Figure 3.12. Morphological analysis conducted by changing carbon source exposure time as 5, 8 and 15 minutes were given in Figure 4.18, Figure 4.19 and Figure 4.20. Figure 4.18 exhibited local changes in the length and diameter of CNTs which was strongly dependent on Fe^{+3} distribution over fiber surface. Figure 4.19 pointed out large CNTs clustered formed by higher carbon source exposure, which could be due to merged CNTs or agglomerated large catalyst particles. SEM micrographs also revealed that CNTs onto the surface of randomly oriented nanofibers were not homogenously distributed, highly dense and extremely long CNTs over nanofiber surface also were detected as in Figure 4.20 .

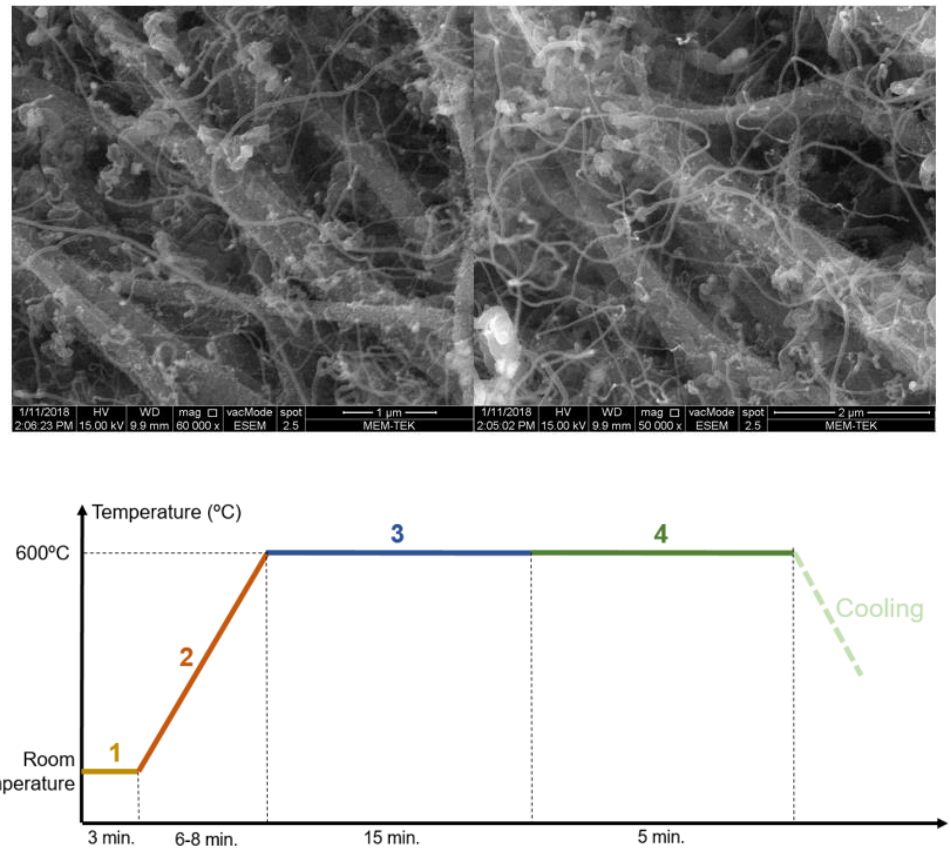

Figure 4.18: (top) SEM micrographs of CNTs grown on randomly oriented PBI nanofibers using 5 minute growth time (bottom) CVD protocol exhibiting time and temperature in each step.

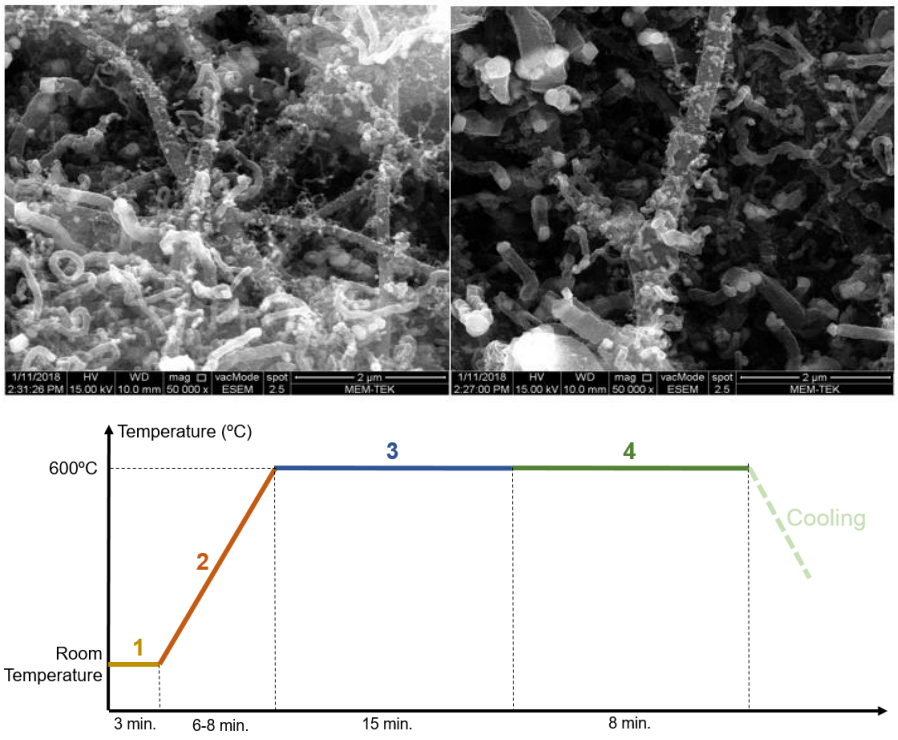

Figure 4.19: (top) SEM micrographs of CNTs grown on randomly oriented PBI nanofibers using 8 minute growth time (bottom) CVD protocol exhibiting time and temperature in each step.

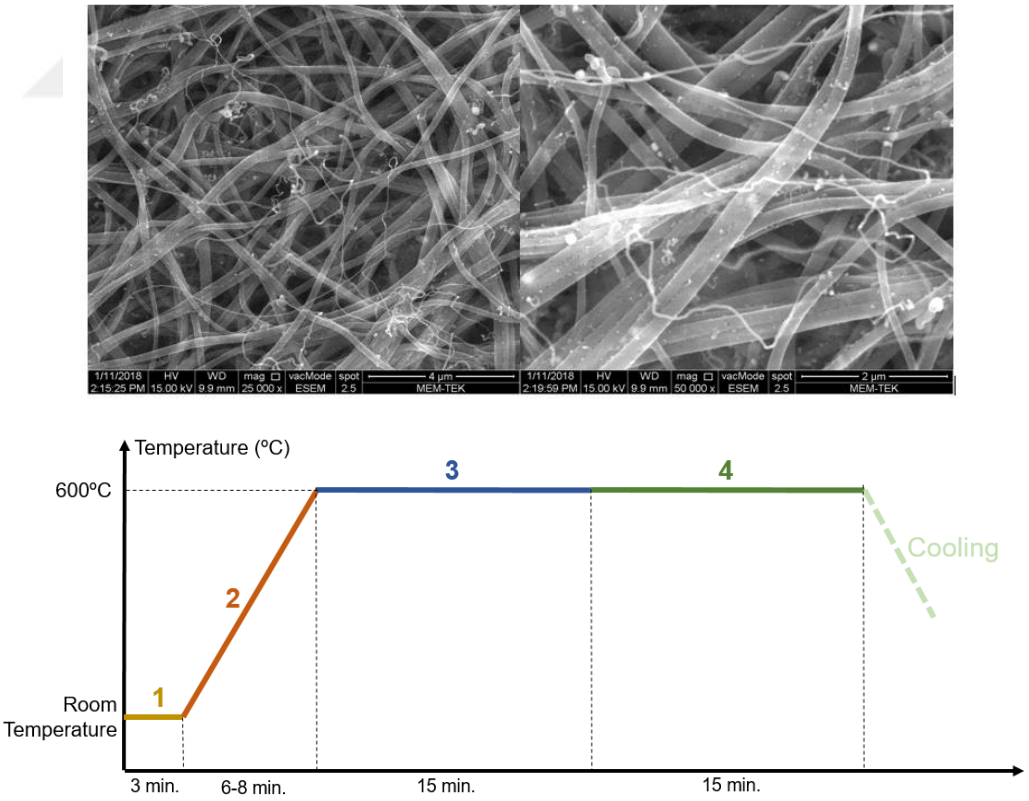

Figure 4.20: (top) SEM micrographs of CNTs grown on randomly oriented PBI nanofibers using 15 minute growth time (bottom) CVD protocol exhibiting time and temperature in each step.

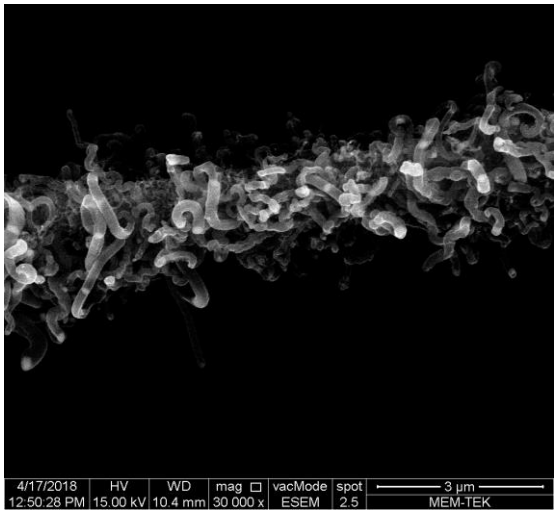

Figure 4.21: CNTs growth onto nanofiber.

Complimentary to randomly oriented PBI nanofibrous substrates, aligned PBI nanofibers could inhibit Fe^{+3} clustering due to induced diffusion at high temperature. Figure 4.21 showed better CNTs coverage compared to the ones in randomly oriented PBI nanofibrous substrates. Besides, nucleation sites were controlled during catalysis, CNTs diameter could be tuned. To measure CNTs diameter, ImageJ software was used Over 20 different CNTs, the average CNTs diameter was measured as 73±19 nm. It is predicted that these diameter variations were associated to the nucleation of iron catalysis onto a curved surface.

4.2.4 Electrical conductivity performance of PBI/CNTs nanocarpets

The electrical conductivity of PBI/CNTs nanocarpets, produced on different nanofibrous substrate were given in Table 4.2. Figure 4.22 showed the dimensions of prepared specimens. The conductivity of CNTs when combined with polymers was directly related to the concentration, alignment, interfacial interaction between nanomaterial and matrix [78]. As it was clear that PBI nanofibers were insulators and did not conduct electrons. CNTs positively contributed to electrical conductivity mechanism and enabled electron transport, as revealed in Table 4.2. The results also showed that randomly oriented PBI/CNTs nanocarpets at different substrates with different fiber diameter had more and less similar conductivity values. However, coarser fiber promoted CNTs irregularities and decreased CNTs quality. Nevertheless, when electrical conduction network was of concern, CNTs interconnectivity defined electrical conductivity. Hence, PBI/CNTs nanocarpets produced at 20wt% with I_G/I_D:

0.96 had highest electrical conductivity. This increase in electrical response could be attributed to the reduction of contact resistance between the nanotubes. Deviation in electrical conductivity between PBI/CNTs nanocarpets produced at 15wt% and 20wt% could be related to the number fraction of CNTs and their coverage. On the other hand, aligned PBI/CNTs produced at 20wt% had better controlled on CNTs orientation, unfortunately, overall behavior was not solely depended on CNTs packing. Hence, 3D network structure of randomly aligned PBI/CNT nanocarpets at 20wt% had higher electrical conductivity.

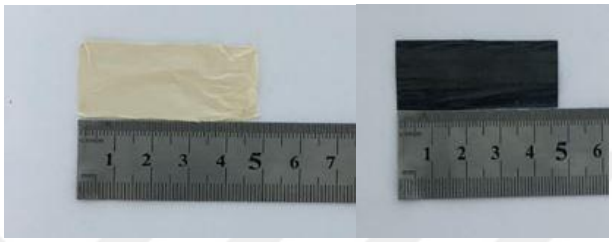

Figure 4.22: (left) PBI nanofiber (right) PBI/CNTs nanocarpet.

Table 4.2: Electrical conductivity results.

Sample	Resistivity (ohm)	Conductivity (S/cm)
PBI Nanofiber	1100.4±55	0.2±0.01
15wt% PBI/CNTs (I_G/I_D:1.16)	61.4±45	1.2.±0.7
20% PBI/CNTs (I_G/I_D:0.96)	55.6±18	4.4±1.5
22% PBI/CNTs (I_G/I_D:0.98)	185.4±84	1.4±0.6
20% Aligned PBI/CNTs	136±54	1.5±0.6

4.2.5 CNTs grown on PBI based commercial fabric

This thesis also explored the possibility of using commercial PBI based yarns and fabrics as substrate to CNTs synthesis. Micron scale coarser yarns and their weaves might be beneficial to control CNTs orientation. Figure 4.23.a demonstrated optical microscope image of commercial fabric with the composition of 59% P-aramid/ 40% PBI/1% anti-static whereas on the right it was revealed the unsuccessful CNTs growth on these fabrics. Same results were also seen in Figure 4.23.b, where had lower aramid content. The results suggested that Fe^{+3} ions were not physically attached to fibers that

led to inhibit CNTs growth onto fiber surface. Hence, yarns were peeled off these fabrics and surface finishing was washed by acetone to improve catalyst deposition.

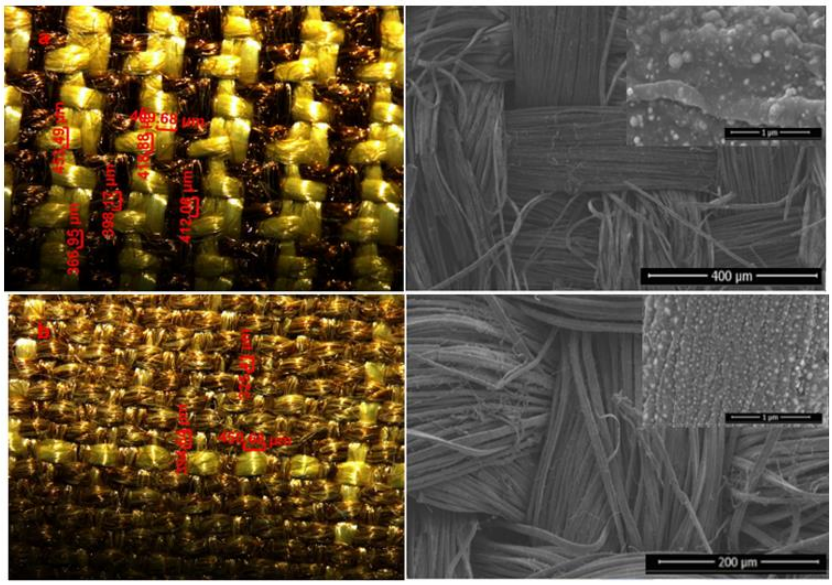

Figure 4.23: a) Optical microscope image of image of commercial fabric with the composition of 59% P-aramid/ 40% PBI/1% anti-static (left), SEM images revealing unsuccessful growth on image of commercial fabric with the composition of 59% P-aramid/ 40% PBI/1% anti-static (right) b) Optical microscope image of image of commercial fabric with the composition of 58% P-aramid/ 40% PBI/2% anti-static (left), SEM images revealing unsuccessful growth on image of commercial fabric with the composition of 58% P-aramid/ 40% PBI/2% anti-static (right).

Figure 4.24.a demonstrated catalyst doped micron scale yarns and Figure 4.24.b showed the surface features after CVD process conducted. It was seen that catalyst layer caused surface cracks on fiber surface and this situation was supported by reference studies in literature [79]. Figure 4.24.b suggested that removing any surface finishing and sizing assisted to CNTs growth by promoting nucleation process.

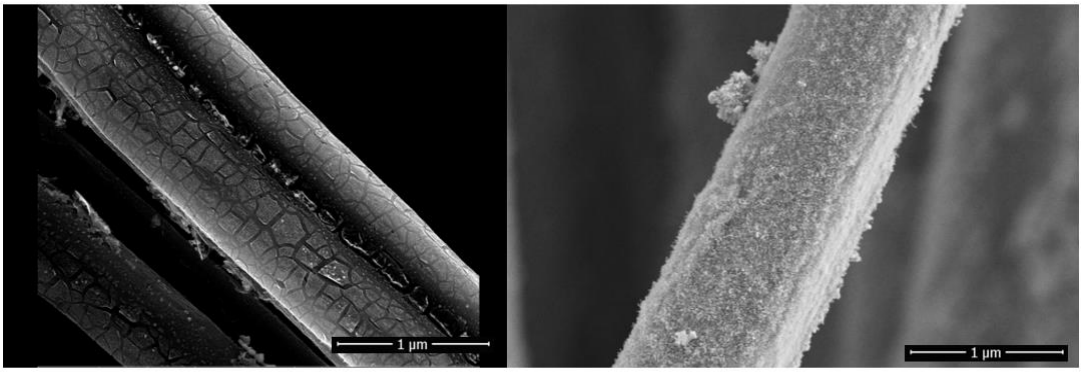

Figure 4.24: SEM images of a) Fe^{+3} doped PBI/Aramid blended fibers b) CNTs grown PBI/Aramid blended fibers.

4.3 Characterization on Thermoplastic Nanoprepregs

4.3.1 Tensile properties

Despite several efforts to reinforce thermoset prepregs [80], in reinforcing thermoplastic laminated composites, there is comprehensive studies needed. When nanomaterials would take a place in reinforcing, several critical factors such as high viscosity and processing temperature would be critical to disperse them into the thermoplastic matrix [81]. The hypothesis was that direct implementation of CNTs onto PBI nanofiber substrates would prevent these issues. Besides, PBI/CNTs nanocarpets when blended with thermoplastic resin would be more practical to be used as interlaminar reinforcement in thermoplastic based laminates. To investigate the mechanical performance of thermoplastic nanoprepregs as a reinforcing element, tensile test was conducted. Tensile test specimens were prepared by laminating PBI nanofibers and PBI/CNTs nanocarpets with PES thin films as depicted in Figure 4.25.

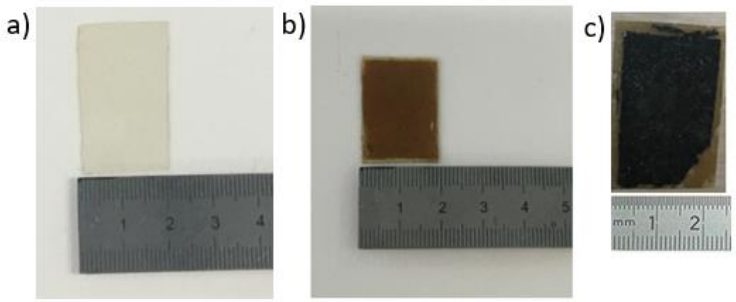

Figure 4.25: a) Neat PES film b) PBI nanofiber interlayered PES nanoprepreg c) PBI/CNTs interlayered PES nanoprepreg.

The preliminary results showed that the tensile strength of PBI/CNTs/PES nanoprepregs with random CNTs distribution was 412±13 MPa, where the tensile strength of PBI/PES nanoprepreg without CNTs was 348±5 MPa as shown in Figure 4.26. Enhancement of tensile strength by approximately 18% was the contribution of CNTs. The increase in tensile performance could be explained by the favorable load transfer mechanism between PES and CNTs and well bonding between CNTs and PES. Not only bonding of outer wall of CNTs with polymer, but also coupling between walls provided better load transfers during tensile loadings [76].

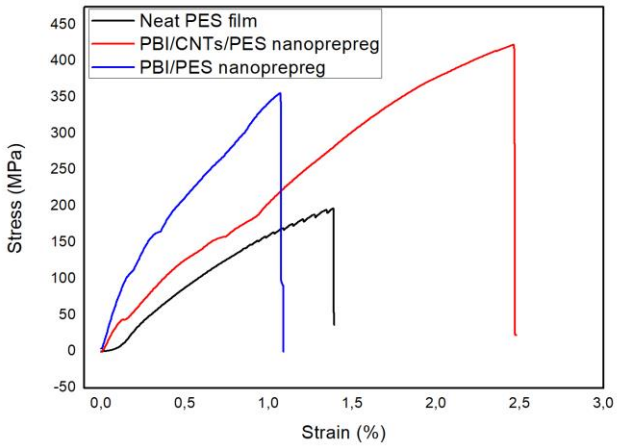

Figure 4.26: Neat PES film, PBI/PES and PBI/CNTs/PES nanoprepreg stress-strain graph.

5. CONCLUSIONS

Thermoplastic nanoprepregs interleaved with CNTs grown PBI nanofibers were successfully fabricated and different characterizations were proved by the following contributions;

- Fabrication of aligned PBI nanofiber with home-built wire drum for the purpose of alignment control of CNTs was achieved. SEM images show the alignment through fiber direction. Optimization in nanofiber polymer concentration was carried out and PBI concentration at 20wt% was found as the most promising concentration for electrospinning of PBI nanofibers, and these fibers were used as a substrate for CNTs growth.
- To obtain a uniform distribution of Fe^{+3} metal ions onto nanofiber, two different catalyze methods as of immersion and dip-coating were performed. There was no clear effect of on CNTs quality depending on the catalysis process. Nevertheless, high purity of CNTs was produced onto nanofiber, as revealed by Ig/Id ratio.
- According to solubility parameters determined by molecular dynamics, PES polymer has higher affinity to PBI polymer, which indicated better wettability and ease on the preparation of thermoplastic nanoprepreg. Hence, PES films were interleaved by PBI/CNTs nanocarpets.
- Mechanical results showed an enhancement in CNTs grown PBI nanofiber interleaved thermoplastic nanoprepregs under tensile loadings. The increase can be attributed both to stronger mechanical interlocking and better load transfer between CNTs and PES resin.
- Preliminary flexure results of the thermoplastic laminated composite which was interleaved with produced thermoplastic nanoprepreg were found as promising for the following studies in the case of interlayer toughening.

REFERENCES

[1] **Díaz, J. and L. Rubio** (2003). Developments to manufacture structural aeronautical parts in carbon fibre reinforced thermoplastic materials. *Journal of Materials Processing Technology 143-144*: 342-346.

[2] **Mastro, P.F.** (2016). Introduction to plastic materials.

[3] **Bilge, K. and M. Papila** (2015). Interlayer toughening mechanisms of composite materials.

[4] **J.-F. Colomer, C.S., S. Lefrant, G. Van Tendeloo, I. Willems, and A.F. Z. Konya, Ch. Laurent, J. B.Nagy** (2000). Large-scale synthesis of single-wall carbon nanotubes by catalytic chemical vapor deposition CCVD/ method. *Chemical Physics Letters 317*: 83-89.

[5] **H. Hongo, M.Y., T. Ichihashi, F. Nihey, S. Iijima** (2002). Chemical vapor deposition of single-wall carbon nanotubes on iron-film-coated sapphire substrates. *Chemical Physics Letters 361*: 349–354.

[6] **Ibrahim, I., et al.** (2011). Optimizing substrate surface and catalyst conditions for high yield chemical vapor deposition grown epitaxially aligned single-walled carbon nanotubes. *Carbon 49*(15): 5029-5037.

[7] **Biron, M.** (2013). Thermoplastic Composites.

[8] **Crouch, I.G.** (2017). Laminated materials and layered structures.

[9] **Díez-Pascual, A.M., et al.** (2010). High performance PEEK/carbon nanotube composites compatibilized with polysulfones-II. Mechanical and electrical properties. *Carbon 48*(12): 3500-3511.

[10] **Kuo, M.C., et al.** (2003). Fabrication of High Performance Magnesium/Carbon-Fiber/PEEK Laminated Composites. *Material Transactions 44*.

[11] **V.Ranatunga and S.Clay** Improvement of Fracture Toughness with Flocking and Z-pinning.

[12] **Mouritz, A.P.** (2007). Review of z-pinned composite laminates. *Composites Part A: Applied Science and Manufacturing 38*(12): 2383-2397.

[13] **Crane, R.M. and J. E.T. Camponeschi** (1986). Experimental and Analytical Characterization of Multidimensionally Braided Graphite/Epoxy Composites. *Experimental Mechanics*.

[14] **Shivakumar, K.N., R. Panduranga, and M. Sharpe** (2013). Interleaved Polymer Matrix Composites - A Review. 54th AIAA/ASME/ASCE/AHS/ASC Structures, Structural Dynamics, and Materials Conference.

[15] **Stevanovic, D.** (2003). Mode I and mode II delamination properties of glass/vinyl-ester composite toughened by particulate modified interlayers. *Composites Science and Technology 63*(13): 1949-1964.

[16] **Yasaee, M., et al.** (2012). Mode I interfacial toughening through discontinuous interleaves for damage suppression and control. *Composites Part A: Applied Science and Manufacturing 43*(1): 198-207.

[17] **Yasaee, M., et al.** (2012). Mode II interfacial toughening through discontinuous interleaves for damage suppression and control. *Composites Part A: Applied Science and Manufacturing 43*(1): 121-128.

[18] **White, K.L. and H.-J. Sue** (2012). Delamination toughness of fiber-reinforced composites containing a carbon nanotube/polyamide-12 epoxy thin film interlayer. *Polymer 53*(1): 37-42.

[19] **Hojo, M., et al.** (2006). Mode I delamination fatigue properties of interlayer-toughened CF/epoxy laminates. *Composites Science and Technology 66*(5): 665-675.

[20] **Greiner, A. and J.H. Wendorff** (2007). Electrospinning: a fascinating method for the preparation of ultrathin fibers. *Angew Chem Int Ed Engl 46*(30): 5670-703.

[21] **Teo, W.E. and S. Ramakrishna** (2006). A review on electrospinning design and nanofibre assemblies. *Nanotechnology 17*(14): R89-R106.

[22] **Sihn, S., et al.** (2008). Improvement of damage resistance in laminated composites with electrospun nano-interlayers. *Composites Science and Technology 68*(3-4): 673-683.

[23] **Zhang, J., T. Lin, and X. Wang** (2010). Electrospun nanofibre toughened carbon/epoxy composites: Effects of polyetherketone cardo (PEK-C) nanofibre diameter and interlayer thickness. *Composites Science and Technology 70*(11): 1660-1666.

[24] **Jiang, S., et al.** (2012). Novel layer-by-layer procedure for making nylon-6 nanofiber reinforced high strength, tough, and transparent thermoplastic polyurethane composites. *ACS Appl Mater Interfaces 4*(8): 4366-72.

[25] **Palazzetti, R., et al.** (2012). Influence of electrospun Nylon 6,6 nanofibrous mats on the interlaminar properties of Gr–epoxy composite laminates. *Composite Structures 94*(2): 571-579.

[26] **Zussman, E., et al.** (2005). Mechanical and structural characterization of electrospun PAN-derived carbon nanofibers. *Carbon 43*(10): 2175-2185.

[27] **Chen, L.S., et al.** (2009). Development of a transparent PMMA composite reinforced with nanofibers. *Polymer Composites 30*(3): 239-247.

[28] **Van der Heijden, S., et al.** (2014). Interlaminar toughening of resin transfer moulded glass fibre epoxy laminates by polycaprolactone electrospun nanofibres. *Composites Science and Technology 104*: 66-73.

[29] **Zhang, J., et al.** (2012). Phase morphology of nanofibre interlayers: Critical factor for toughening carbon/epoxy composites. *Composites Science and Technology 72*(2): 256-262.

[30] **Brugo, T., et al.** (2017). Study on Mode I fatigue behaviour of Nylon 6,6 nanoreinforced CFRP laminates. *Composite Structures 164*: 51-57.

[31] **Beckermann, G.W. and K.L. Pickering** (2015). Mode I and Mode II interlaminar fracture toughness of composite laminates interleaved with electrospun nanofibre veils. *Composites Part A: Applied Science and Manufacturing 72*: 11-21.

[32] **Saghafi, H., et al.** (2015). Influence of electrospun nanofibers on the interlaminar properties of unidirectional epoxy resin/glass fiber composite laminates. *Journal of Reinforced Plastics and Composites 34*(11): 907-914.

[33] **Bilge, K., et al.** (2012). Structural composites hybridized with epoxy compatible polymer/MWCNT nanofibrous interlayers. *Composites Science and Technology 72*(14): 1639-1645.

[34] **Nuhiji, B., et al.** (2011). The effect of alternate heating rates during cure on the structure–property relationships of epoxy/MMT clay nanocomposites. *Composites Science and Technology 71*(15): 1761-1768.

[35] **Ye, Y., et al.** (2011). Interlaminar properties of carbon fiber composites with halloysite nanotube-toughened epoxy matrix. *Composites Science and Technology 71*(5): 717-723.

[36] **Iijima, S.** (1991). Helical microtubules of graphitic carbon. *Nature 354*.

[37] **Liu, L., W. Ma, and Z. Zhang** (2011). Macroscopic carbon nanotube assemblies: preparation, properties, and potential applications. *Small 7*(11): 1504-20.

[38] **Sathyanarayana, S. and C. Hübner** (2013). Thermoplastic Nanocomposites with Carbon Nanotubes.

[39] **José-Yacamán, M., et al.** (1993). Catalytic growth of carbon microtubules with fullerene structure. *Applied Physics Letters 62*(6): 657-659.

[40] **Chin Li Cheung, A.K., Hongkun Park, and Charles M. Lieber** (2002). Diameter-Controlled Synthesis of Carbon Nanotubes. *The Journal of Physical Chemistry B 106*: 2429-2433.

[41] **Kenji Hata, D.N.F., Kohei Mizuno, Tatsunori Namai, and S.I. Motoo Yumura** (2004). Water-Assisted Highly Efficient Synthesis of Impurity-Free Single-Walled Carbon Nanotubes. *Science 306*.

[42] **I. Willems, Z.K.n., J.-F. Colomer, G. Van Tendeloo, N. Nagaraju, and J.B.N. A. Fonseca** (2000). Control of the outer diameter of thin carbon nanotubes synthesized by catalytic decomposition of hydrocarbons. *Chemical Physics Letters* 71-76.

[43] **Kumar, M. and Y. Ando** (2003). A simple method of producing aligned carbon nanotubes from an unconventional precursor – Camphor. *Chemical Physics Letters 374*(5-6): 521-526.

[44] **Yamamoto, N., et al.** (2009). High-yield growth and morphology control of aligned carbon nanotubes on ceramic fibers for multifunctional enhancement of structural composites. *Carbon 47*(3): 551-560.

[45] **Mathur, R.B., S. Chatterjee, and B.P. Singh** (2008). Growth of carbon nanotubes on carbon fibre substrates to produce hybrid/phenolic composites with improved mechanical properties. *Composites Science and Technology 68*(7-8): 1608-1615.

[46] **N. Nagaraju, A.F., Z. Konyac, J.B. Nagy** (2002). Alumina and silica supported metal catalysts for the production of carbon nanotubes. *Journal of Molecular Catalysis A: Chemical 181*: 57–62.

[47] **Lee, W.Y., et al.** (2004). Patterned aligned growth of carbon nanotubes on porous structure templates using chemical vapor deposition methods. *Diamond and Related Materials 13*(4-8): 1232-1236.

[48] **Robert Seidel, G.S.D., Eugen Unger, Andrew P. Graham, Maik Liebau, and Franz Kreupl** (2004). Chemical Vapor Deposition Growth of Single-Walled Carbon Nanotubes at 600 °C and a Simple Growth Model. *The Journal of Physical Chemistry B 108*.

[49] **Randall L. Vander Wal , T.M.T., Valerie E. Curtis** (2001). Substrate–support interactions in metal-catalyzed carbon nanofiber growth. *Carbon 39*: 2277–2289.

[50] **Kumar, M. and Y. Ando** (2010). Chemical Vapor Deposition of Carbon Nanotubes: A Review on Growth Mechanism and Mass Production. *Journal of Nanoscience and Nanotechnology 10*(6): 3739-3758.

[51] **Qian, H., et al.** (2010). Carbon nanotube-based hierarchical composites: a review. *Journal of Materials Chemistry 20*(23): 4751.

[52] **Garcia, E., et al.** (2008). Fabrication and multifunctional properties of a hybrid laminate with aligned carbon nanotubes grown In Situ. *Composites Science and Technology 68*(9): 2034-2041.

[53] **Díez-Pascual, A.M., et al.** (2011). Influence of carbon nanotubes on the thermal, electrical and mechanical properties of poly(ether ether ketone)/glass fiber laminates. *Carbon 49*(8): 2817-2833.

[54] **Shen, Z., et al.** (2009). The effects of carbon nanotubes on mechanical and thermal properties of woven glass fibre reinforced polyamide-6 nanocomposites. *Composites Science and Technology 69*(2): 239-244.

[55] **Rausch, J. and E. Mäder** (2010). Health monitoring in continuous glass fibre reinforced thermoplastics: Manufacturing and application of interphase sensors based on carbon nanotubes. *Composites Science and Technology 70*(11): 1589-1596.

[56] **Rausch, J. and E. Mäder** (2010). Health monitoring in continuous glass fibre reinforced thermoplastics: Tailored sensitivity and cyclic loading of CNT-based interphase sensors. *Composites Science and Technology 70*(13): 2023-2030.

[57] **Qian, H., et al.** (2010). Carbon nanotube grafted carbon fibres: A study of wetting and fibre fragmentation. *Composites Part A: Applied Science and Manufacturing 41*(9): 1107-1114.

[58] **Rahmanian, S., et al.** (2013). Carbon and glass hierarchical fibers: Influence of carbon nanotubes on tensile, flexural and impact properties of short fiber reinforced composites. *Materials & Design 43*: 10-16.

[59] **Veedu, V.P., et al.** (2006). Multifunctional composites using reinforced laminae with carbon-nanotube forests. *Nat Mater 5*(6): 457-62.

[60] **Díez-Pascual, A.M.** (2017). Hybrid carbon nanotube/fiber thermoplastic composites.

[61] **Khan, S.U. and J.-K. Kim** (2012). Improved interlaminar shear properties of multiscale carbon fiber composites with bucky paper interleaves made from carbon nanofibers. *Carbon 50*(14): 5265-5277.

[62] **Wang, Y., et al.** (2015). Polybenzimidazoles.

[63] **Jong-Sang, K. and D.H. Reneker** (1999). Polybenzimidazole Nanofiber Produced by Electrospinning. *Polymer Engineering and Science 39*.

[64] **Weber, J.** (2010). Nanostructured poly(benzimidazole): from mesoporous networks to nanofibers. *ChemSusChem 3*(2): 181-7.

[65] **Lai, S., et al.** (2016). Mechanical property enhancement of ultra-thin PBI membrane by electron beam irradiation for PEM fuel cell. *International Journal of Hydrogen Energy 41*(22): 9556-9562.

[66] **Von Graberg, T., et al.** (2008). Electrospun Silica-Polybenzimidazole Nanocomposite Fibers. *Macromolecular Materials and Engineering 293*(10): 815-819.

[67] **Garg, K. and G.L. Bowlin** (2011). Electrospinning jets and nanofibrous structures. *Biomicrofluidics 5*(1): 13403.

[68] **Širc, J., et al.** (2012). Morphological Characterization of Nanofibers: Methods and Application in Practice. *Journal of Nanomaterials 2012*: 1-14.

[69] **Corcione, C. and M. Frigione** (2012). Characterization of Nanocomposites by Thermal Analysis. *Materials 5*(12): 2960-2980.

[70] **Belin, T. and F. Epron** (2005). Characterization methods of carbon nanotubes: a review. *Materials Science and Engineering: B 119*(2): 105-118.

[71] **Herrero-Latorre, C., et al.** (2015). Characterization of carbon nanotubes and analytical methods for their determination in environmental and biological samples: a review. *Anal Chim Acta 853*: 77-94.

[72] **Tong, H.-W. and M. Wang** (2011). An investigation into the influence of electrospinning parameters on the diameter and alignment of poly(hydroxybutyrate-co-hydroxyvalerate) fibers. *Journal of Applied Polymer Science 120*(3): 1694-1706.

[73] **P. Katta, et al.** (2004). Continuous Electrospinning of Aligned Polymer Nanofibers onto a Wire Drum Collector. *NanoLetters 4*: 2215-2218.

[74] **Gooch, J.W.** (2007). Encyclopedic Dictionary of Polymers of Entry. Encyclopedic Dictionary of Polymers of WebLog Accessed Access 2007.

[75] **Wu, G.-P., et al.** (2009). Comparative investigation on the thermal degradation and stabilization of carbon fiber precursors. *Polymer Bulletin 62*(5): 667-678.

[76] **Schadler, L.S., S.C. Giannaris, and P.M. Ajayan** (1998). Load transfer in carbon nanotube epoxy composites. *Applied Physics Letters 73*(26): 3842-3844.

[77] **Dupuis, A.** (2005). The catalyst in the CCVD of carbon nanotubes—a review. *Progress in Materials Science 50*(8): 929-961.

[78] **Erik T. Thostenson, Z.R., Tsu-Wei Choua** (2001). Advances in the science and technology of carbon nanotubes and their composites: a review. *Composite Science and Technology 61*: 1899–1912.

[79] **Paukner, C. and K.K. Koziol** (2014). Ultra-pure single wall carbon nanotube fibres continuously spun without promoter. *Sci Rep 4*: 3903.

[80] **Ashrafi, B., et al.** (2011). Enhancement of mechanical performance of epoxy/carbon fiber laminate composites using single-walled carbon nanotubes. *Composites Science and Technology 71*(13): 1569-1578.

[81] **Castillo, F.Y., et al.** (2011). Electrical, mechanical, and glass transition behavior of polycarbonate-based nanocomposites with different multi-walled carbon nanotubes. *Polymer 52*(17): 3835-3845.

CURRICULUM VITAE

Name Surname **:** Beyza BOZALİ

Place and Date of Birth **:** TRABZON/23.08.1989

E-Mail **:** bozali@itu.edu.tr

EDUCATION:

B.Sc. : Textile Engineering/ITU

EXPERIENCE:

2016-2018 : TUBITAK 116M427 Project Researcher

2016 – 2018 : ITU-SAFRAN R&D Project Researcher Scholar

PUBLICATIONS, PRESENTATIONS AND PATENTS ON THE THESIS

"CNTs growth on polymeric nanofibers as interleaves for thermoset composites", **Bozali B.**, Cebeci H., and Ozden Yenigün E., 3rd International Conference on Mechanics of Composites, 4-7 July 2017, Bologna, ITALY/ Oral Presentation

"Synthesis of Boron Nitride Nanotubes on Silicon Carbide Fibers and Investigation of the Mechanical Properties", Köken D., Top A., Cebeci H., **Bozali B.**, Ozden Yenigün E., Cebeci F., Material Research Society, 2017, November 26-December 1, Boston Massachusetts, USA / Poster Presentation